Catchment power and the joint distribution of elevation and travel distance to the outlet.

Leonard S. Sklar[1], Clifford S. Riebe[2], Claire E. Lukens[2], Dino Bellugi[3]

[1]Department of Earth and Climate Sciences, San Francisco State University, San Francisco, CA 94132 USA
[2]Department of Geology and Geophysics, University of Wyoming, Laramie, WY 82071 USA
[3]Department of Earth, Atmospheric and Planetary Sciences, MIT, Cambridge, MA 02139 USA

Correspondence to L.S. Sklar (leonard@sfsu.edu)

Abstract The delivery of water, sediment and solutes by catchments is influenced by the distribution of source elevations and their travel distances to the outlet. For example, elevation affects the magnitude and phase of precipitation, as well as the climatic factors that govern rock weathering, which influence the production rate and initial particle size of sediments. Travel distance, in turn, affects the timing of flood peaks at the outlet and the degree of sediment size reduction by wear, which affects particle size distributions at the outlet. The distributions of elevation and travel distance have been studied extensively but separately, as the hypsometric curve and width function. Yet a catchment can be considered as a collection of points, each with paired values of elevation and travel distance. For every point, the ratio of elevation to travel distance defines the mean slope for transport of mass to the outlet. Recognizing that mean slope is proportional to the average rate of loss of potential energy by water and sediment during transport to the outlet, we use the joint distribution of elevation and travel distance to define two new metrics for catchment geometry: "source-area power," and the corresponding catchment-wide integral "catchment power." We explore patterns in source-area and catchment power across three study catchments spanning a range of relief and drainage area. We then develop an empirical algorithm for generating synthetic source-area power distributions, which can be parameterized with data from natural catchments. This new way of quantifying the three-dimensional geometry of catchments can be used to explore the effects of topography on the distribution on fluxes of water, sediment, isotopes and other landscape products passing through catchment outlets, and may provide a fresh perspective on problems of both practical and theoretical interest.

1. Introduction

The physical and ecological dynamics of rivers are influenced by upstream sources of water, solutes, and sediment. These materials are produced at rates that vary from source to source depending on factors such as precipitation, weathering, erosion, and ecosystem productivity. Spatial variations in these factors commonly correspond to differences in elevation. For example, elevation influences both the magnitude and phase of precipitation (Roe, 2005; Minder et al., 2011), the climatic factors that govern rock weathering (White and Blum, 1995; Riebe et al., 2004), the particle size and production rate of sediment from slopes (Marshall and Sklar, 2012; Riebe et al., 2015; Sklar et al., 2016), and both the distribution of

biomes (Lomolino, 2001) and their net primary productivity (Raich et al., 1997). Thus elevation is a fundamental characteristic of the source areas that supply water, solutes, and sediment to catchment outlets.

Along the journey from source to outlet, material is mixed together with products of other sources and altered by chemical, physical, and biological processes. The mixing and alteration of materials depends in part on the travel distance between the source and outlet. For example, travel distance influences the generation of flood waves (Richie et al., 1989), the liberation of solutes and nutrients from soil and sediment (Gaillardet et al., 1999; Jin et al., 2010), the physical breakdown of sediment in streams (Attal and Lave, 2006), and the decomposition of organic matter (Taylor and Chauvet, 2014). Thus travel distance is another fundamental aspect of the link between source and outlet for water, solutes, sediment, and nutrients.

Together, the effects of elevation and travel distance should govern the amount, timing, and composition of fluxes from catchments. However, previous work has explored the distributions of elevation and travel distance separately, without consideration of their joint distribution. The distribution of elevations – known as hypsometry – reveals the vertical structure of a catchment and has been used to quantify landscape development, identify geomorphic process regimes, and understand the sensitivity of land area to changes in sea level (Strahler, 1952; Lifton and Chase, 1992; Brozovic et al., 1997; Brocklehurst and Whipple, 2004; Algeo and Seslavinsky, 1995). Meanwhile, the distribution of travel distances – known as the width or area function – reveals the horizontal structure of catchments and has been used to characterize catchment shape, identify channel branching structure, and understand hydrographs (Gupta and Mesa, 1988; Rinaldo et al., 1995; Sklar et al., 2006; Moussa, 2008; Rigon et al., 2015).

Although both the hypsometry and width functions of catchments have been widely studied, to our knowledge elevation and travel distance have only been considered together in an analysis of the hypsometry of channel network links (Gupta and Waymire, 1989) and in plots of longitudinal profiles of trunk streams and tributaries (Rigon et al., 1994). Thus, previous research has overlooked the insights that might be gained by analyzing hillslopes and channels together as a collection of paired values of elevation and travel distance. Some questions that might be addressed by such an analysis include: Which if any aspects of the joint distribution of elevation and travel distance are common from one catchment to the next? What are the most revealing measures of differences in the distributions across different catchments? Do the distributions differ in ways that systematically reflect the factors that drive landscape evolution, such as weathering, climate, and tectonics?

Here we address these questions using topographic data from three catchments of differing area and relief. First we explore how the distributions of elevation and travel distance vary across our study catchments. Then we show how elevation and travel distance can be combined into a single quantity, referred to here as catchment power because it expresses the rate of potential energy dissipation of water and sediment as they travel from source locations to the catchment outlet. Next, using our analyses of the elevation and travel distance distributions from the study catchments, we develop an approach for

generating synthetic catchments that capture many features of power distributions in natural landscapes. Finally, we discuss how this approach can be used to explore how factors such as area, relief, and profile concavity influence catchment power and more broadly how rivers are influenced by hillslope sources of water, solutes, and sediment (e.g. Lukens et al., 2016).

2. Elevation and travel distance in natural landscapes

To explore how joint distributions of elevation and travel distance vary in natural landscapes, we chose catchments drained by Inyo Creek, Providence Creek, and the Noyo River, all in California, USA (Fig. 1). Each of these catchments has been featured in previous studies of the production and delivery of water, solutes, and sediment from slopes to channels. Thus our selection of sites allows us to link analyses of elevation and travel distance distributions to existing research on physical, chemical, and biological processes in the catchments. All of the catchments are developed in mountain landscapes, where the products of runoff, weathering, and erosion reach the outlet without any long-term interception in floodplains or lakes; thus, the travel distance distributions should strongly reflect transport processes in the catchments. At each site, we extracted elevations from a 10-m digital elevation model (DEM) and calculated travel distance to the outlet using a steepest descent algorithm (Tarboton, 1997). The catchments span a range in relief, drainage area, and mean slope (Table 1), and thus also a range in the populations of paired values of elevation and travel distance (Fig. 1).

2.1 Study sites

The Inyo Creek catchment spans 2 km of relief over 4 km of travel distance on the eastern slope of the High Sierra (Table 1). Unlike some of its neighboring catchments along the range, it has never been scoured by glaciers, making it ideal for comparison of sediment production and landscape evolution in glaciated and non-glaciated terrain (Riebe et al., 2015; Stock et al., 2006; Brocklehurst and Whipple, 2002). Moreover, the catchment spans a range in the relative importance of physical, chemical, and biological weathering from its warm, gently sloped, low elevations to its cold, steep headwaters.

On the other side of the Sierra Nevada, Providence Creek spans 1 km of relief over 8 km of travel distance (Table 1). This catchment is part of the Southern Sierra Critical Zone Observatory, which has been the focus of numerous recent studies of hydrology, biogeochemistry, and geomorphology (e.g., Bales et al., 2011; Hunsaker and Neary, 2012; Hunsaker et al., 2012; Goulden and Bales, 2014; Holbrook et al., 2014; Hahm et al., 2014). Precipitation in the upper half of the catchment dominantly falls as snow, whereas precipitation in the lower half dominantly falls as rain. Unlike the roughly continuous concave ridge and channel profiles of Inyo Creek, catchment topography in Providence Creek exhibits a pronounced step in elevation of both the channel and ridge profiles (Fig. 1). Steps like these, which are common on the southwestern slope of the Sierra Nevada, have been interpreted to reflect a feedback between weathering and erosion (Wahrhaftig, 1965).

Farther to the northwest, in the California Coast Ranges, the Noyo River catchment spans 0.9 km of relief over 20 km of travel distance. Thus the catchment is significantly larger and more gently sloped on average than either of the other two study catchments. The catchment has a long history of intensive timber harvests and has been the site of numerous studies of the effects of land use on in-stream habitat (Burns, 1972; Lisle, 1982; Leithold et al., 2006;) and the role of topography and channel network structure in the production and delivery of sediment from slopes to channels (Dai et al., 2004; Sklar et al., 2006).

2.2 Spatial distributions of elevation and travel distance

The maps in Figure 2 show the spatial distributions of elevation and travel distance across each catchment. Broadly, travel distance and elevation covary in space; the highest elevations in each catchment tend to be further away from the outlet. However, in detail, elevation contours are not aligned with contours of equal travel distance; in general the elevation contours exhibit higher planform curvature than travel distance contours. This pattern is especially clear at Inyo Creek (Fig. 2a) and Providence Creek (Fig. 2b), which drain small, relatively undissected catchments. In particular, as can be seen in Fig. 2a by following a given elevation contour (black lines), travel distances (color bands) are longest in the valley axis and shortest at the ridges. Conversely, for a given travel distance (i.e. following a boundary between color bands), elevations are highest at the ridges and lowest in the valley axis.

The patterns in elevation and travel distance in the Noyo River catchment are more complex (Fig. 2c), in part because it is more deeply incised by multiple high-order trunk streams. At ridges that separate these trunk streams, travel distance can vary considerably from one side of the ridge to the other. Thus nearby points that share the same elevation can have very different travel distances. For example, along the central ridge, which runs along the catchment's axis, points on the south side of the ridge drain to a more sinuous and thus longer southern trunk stream, giving them longer travel distances to the outlet than points on the northern side. For the same travel distance, points occur at higher elevations in the sub-catchment of the northern, less sinuous trunk stream.

2.3 Hypsometry and the width function

The spatial patterns shown in the maps are reflected in both the hypsometry and the width function, which are the conventional ways of displaying distributions of elevation and travel distance separately (Fig. 3). For example, hypsometry shows that most of the Inyo Creek catchment area occurs at mid elevations (Fig. 3a), because the catchment narrows both at low elevation near the outlet and at high elevation near the catchment divide (Fig. 2a). This differs from the hypsometry of Providence Creek, where most of the catchment area occurs at higher elevations, above the pronounced step in the topography. Meanwhile, at the Noyo River site, the majority of area occurs at lower elevations, because the catchment is deeply dissected, with wide valley bottoms and steep, narrow ridges.

140 Hypsometry reveals differences in the vertical structure of the catchments, whereas the width
141 function reveals differences in planform structure, which are governed in part by differences in the shapes
142 of the catchment boundaries. For example, the distribution of travel distances at Inyo Creek is symmetrical,
143 reflecting the roughly oval shape of the catchment. Meanwhile, at Providence Creek, the distribution of
144 travel distances is bimodal, reflecting the narrowing near the middle of the catchment. At the Noyo River
145 site, the travel-distance distribution is skewed, with the majority of the area at long travel distances,
146 reflecting the widening of the catchment with increasing distance from the outlet that is evident in Figure
147 2c.

148 **2.4 Joint distributions of elevation and travel distance**

149 Figure 3 shows that much can be learned from the distributions of elevation and travel distance
150 plotted alone. However, they do not reveal information contained in the distribution of paired values of
151 elevation and travel distance. One potentially insightful index that can be missed is the ratio of elevation to
152 travel distance, which is the mean slope for water, solutes, and sediment on a path of steepest descent from
153 source to outlet. The ranges in elevations and travel distances from these three catchments imply that the
154 distribution of mean slopes differ markedly across our sites (Table 1; Fig. 1). These differences likely
155 correspond to differences in factors such as water-transit times, sediment breakdown rates, and channel
156 morphology. Although information on the distribution of mean slopes is embedded in both the hypsometry
157 and the width function, it cannot be extracted from either of them plotted alone or even plotted side by side
158 (Fig. 3).
159 To overcome the limitations of separate plots of vertical and horizontal structure, we plotted the
160 joint distribution of elevation and travel distance for every point in each of the catchments in Figure 4.
161 These plots show both the long profile of the channel network and the distribution of hillslope sources,
162 which account for more than 98% of the source area in each catchment. A number of similarities emerge
163 across the sites (Fig. 4a-c). Strikingly, at the highest elevations for any given travel distance, sources are
164 aligned in steeply-sloped tendrils of data that coalesce at lower elevations. These tendrils represent hillslope
165 sources aligned along common flow paths that cluster together into narrow groups. Equally striking are the
166 gaps between the tendrils, which represent paired values of elevation and travel distance that do not occur
167 anywhere in the catchment. Meanwhile, many paired values are so common that they overlap, particularly
168 along flowpaths that converge near the mainstem channel.
169 Bivariate frequency distributions help shed light on the degree of clustering and overlap of data at
170 shared values (Fig. 4 d-f). These binned representations of the raw data show that, for a given travel
171 distance, the lowest point densities (point area = 100 m^2) generally occur at the highest relative elevations.
172 As relative elevation decreases within a vertical stack of data, point density typically increases to a peak
173 and then approaches zero at the channel elevation. In general, peak densities for a given travel distance
174 occur closer to the channel than the ridge elevation, although there are notable exceptions. Figure 4 (d-f)

also shows that the greatest frequency of the high point density (normalized density > 0.6) primarily occurs in the upper third of Inyo and Providence Creeks, and in the upper half of Noyo Creek.

These patterns in the density of paired values of elevation and travel distance help explain the shapes of the corresponding hypsometry and width functions. For example, Figure 3 shows that in the Noyo Creek catchment the majority of area occurs at relatively long travel distances and relatively low elevations. Yet Figure 4f shows that this does not mean that the highest densities of catchment area occur at points that have both long travel distance and low elevation. Rather, low elevations dominate across all travel distances, and summing area horizontally across figure 4f leads to higher total area in the lower elevation bins of Figure 3a. Similarly, the Noyo catchment has greater relief at longer travel distances, and summing area vertically across fig. 4f leads to higher total area in the longer travel distance bins of Figure 3b. This comparison demonstrates that the joint distribution of elevation and travel distance reveals where area is distributed in the vertical and horizontal structure of the catchment in ways that the hypsometry and width function cannot.

Comparisons of the joint distributions between catchments also reveals significant differences that cannot be inferred from the conventional representations of vertical and horizontal catchment structure in Fig. 3. For example, the relative slopes of the tendrils and the channels differ markedly. The tendrils are much steeper than the mainstem channel profile in the Noyo River catchment (Fig. 4f). Conversely, in the other two catchments, the tendrils and the main channel profile have similar slopes, especially at Providence Creek. These differences likely arise at least in part due to the difference in scale of the watersheds; in the Noyo River catchment, some of the individual tendrils encompass large areas, similar in scale to the entire Inyo and Providence Creek catchments. Thus we interpret the tendrils along the Noyo River to be tributary catchments that are similar to the Inyo and Providence Creek catchments, with tendrils of their own that are only slightly steeper than the local tributary channel slopes.

Perhaps the most striking difference among the catchments can be seen in the distributions of mean slope along the travel path to the outlet, which we calculate as the ratio of the paired values of elevation and travel distance (Fig. 5a-c insets). Swaths of common mean slope appear as linear trends through the joint distributions of elevation and travel distance (Fig. 5a-c), or as contours on a planform view of the catchment (Fig. 5d-f). In each catchment the contours of mean slope (Fig. 5d-f) differ markedly from the contours of elevation and travel distance (Fig. 2). Mean slopes are relatively steep and span a relatively narrow range at Inyo Creek (Fig. 5c) compared to the Noyo River catchment (Fig. 5f). Providence Creek is distinguished by a peak in mean slopes (Fig. 5b) corresponding to the upper half of catchment, above the step in the topography (Fig. 5e).

Mean slope quantifies the ratio between elevation and travel distance, and thus is a single metric that combines two fundamental attributes of source areas in catchments. The distributions of source elevation, travel distance, and thus mean slope are ultimately set by the erosion and transport processes that produce and deliver sediment from slopes to channels. Thus spatial variations in mean slope, such as those

shown in Fig. 5, may be closely linked to spatial variations in the production and delivery of water, solutes, and sediment.

3 Source-area and catchment power

To develop a mechanistic framework for linking distributions of source-area mean slope with catchment processes, we introduce the concept of source-area power, which combines elevation, travel distance, and the production rate of material on slopes. In the derivation that follows, we consider a mass (M) of transportable material (such as water, solutes, or sediment) produced at a source elevation z and delivered downstream to an elevation z_o at the catchment outlet. The potential energy (E) of the material at the source, relative to the outlet is given by Equation 1:

$$E_{i,j} = M_{i,j} g R_i = \rho_{i,j} A_i h_{i,j} g \left(z_i - z_o \right) \quad (1).$$

Here g is acceleration due to gravity, R is relief (i.e., the difference in elevation between the source and outlet), ρ is density, h is the thickness of the material produced at the source, A is the area of the source (one pixel in a DEM), the subscript i refers to the specific source location on the slope, and the subscript j refers to the type of material (e.g., water, solutes, or sediment). In the case of solutes, h refers to the equivalent thickness of chemical erosion needed to account for the mass loss due to production of solutes.

At each source, potential energy is produced at a rate (Ω) that is proportional to the production rate (Q) or flux of material from the source, as shown in Equation 2:

$$\Omega_{i,j} = Q_{i,j} g R_i = \rho_{i,j} A_i \frac{\partial h_{i,j}}{\partial t} g \left(z_i - z_o \right) \quad (2).$$

Here, the definition of $\partial h/\partial t$ (in dimensions of length per time) depends on the process considered. For water produced by precipitation, $\partial h/\partial t$ is the precipitation rate. For sediment produced by erosion, $\partial h/\partial t$ is the physical erosion rate. For solutes produced by chemical erosion, $\partial h/\partial t$ is the equivalent to the chemical erosion rate. In all cases, Ω has dimensions of power.

On its journey to the outlet, the material loses its potential energy. This energy is converted to kinetic energy and is primarily lost to heat due to friction. In the case of sediment, some of the energy is consumed when particles are abraded and shattered during collisions with other particles and the channel bed. Thus it may be useful in the context of geomorphic work to think of the power expended by the water or sediment over the travel distance (L) between the source and outlet, as shown in Equation 3:

$$\omega_{i,j} = \frac{Q_{i,j} g R_i}{L_i} = \rho_{i,j} A_i \frac{\partial h_{i,j}}{\partial t} g \frac{\left(z_i - z_o \right)}{L_i} \quad (3).$$

Here ω is the source-area power, which has dimensions of power per length, and $(z_i\text{-}z_o)/L_i$ is the mean slope along the travel path from the source to outlet.

Source-area power is distinct from stream power, which is how energy dissipation in landscapes is

commonly quantified (Rodriguez-Itrube et al., 1992; Lague, 2014). Stream power uses the entire upstream contributing area to calculate the material flux, whereas the contributing area for source-area power is limited to the smallest unit of analysis, such as a single pixel in a DEM. Moreover, stream power quantifies the local rate of energy dissipation across a short distance, such as a reach of river represented by the distance between two pixels, whereas source-area power averages energy dissipation over the entire travel distance from source to catchment outlet. Hence, unlike stream power, source-area power quantifies the production rate of material potential energy in terms of the position of the source location relative to the catchment outlet. This provides a distinct metric for analyzing spatial patterns in how energy is produced and dissipated within catchments.

The concept of source-area power allows us to explore the possible implications of variability in the ratio of elevation to travel distance (i.e., the mean slope) on the production and delivery of water, solutes, and sediment across catchments. For example, in landscapes where the rate of precipitation or erosion is spatially uniform, we expect the distribution of source-area power for the water or sediment to be identical to the distribution of the mean slopes of source areas. In contrast, in landscapes where rates of precipitation and erosion are spatially variable and sometimes correlated (Reiners et al., 2003;, Burbank et al. 2003), we expect the distributions of power and mean slopes to differ. This is the case at Inyo Creek where mean annual precipitation increases with elevation from 290 mm yr^{-1} at the outlet to 710 mm yr^{-1} at the catchment divide (Prism Climate Group, 2014), and the rate of production of sediment by erosion has been estimated to increase exponentially with elevation from 0.03 mm yr^{-1} at the outlet to 1.5 mm yr^{-1} at the divide (Riebe et al., 2015). When we combine these relationships for water and sediment production with the distribution of mean slopes using Equation 3, we can create histograms and maps showing the distributions of source-area power for the two materials, water and sediment (Fig. 6a-b). For both materials, the shape of the distributions shift from negative skew to positive skew, and the power contours are stretched towards the catchment divide, relative to the case of uniform precipitation and erosion (equivalent to Fig. 5a). The difference is greatest for the case of spatially varying erosion (Fig. 6b), due to the nonlinear relationship between erosion rate and elevation. Thus for catchments with spatial variation in the rate of production of water or sediment, mean slope distributions cannot reliably predict distributions of source-area power.

Comparisons of source-area power and production rates for different materials may provide insight into the spatial variation of catchment processes. For example, sediment produced by erosion at source areas is transported to the outlet by a combination of primarily gravity-driven processes, including creep and landslides, and by water-mediated processes such as overland, debris, and fluvial flows. Catchment topography, as expressed in the joint distribution of elevation and travel distance, may reflect the spatial variation and relative importance of these different processes. Because the altitudinal gradients in erosion and precipitation at Inyo Creek are known, we can use them to explore how the source-area power of water, relative to the amount of sediment that must be produced on hillslopes and transported to

the outlet, varies across the catchment assuming steady state. We define a dimensionless ratio ($\omega^*_{i,w/s}$) that quantifies the source-area power of water per mass of sediment eroded at an individual pixel, *i*:

$$\omega^*_{i,w/s} = \frac{\omega_{i,w}}{gQ_{i,s}} = \frac{\rho_w \left(\partial h_{i,w}/\partial t\right)}{\rho_s \left(\partial h_{i,s}/\partial t\right)} \frac{\left(z_i - z_o\right)}{L_i} \quad (4)$$

Here the subscript *w* refers to water produced from precipitation, and the subscript *s* refers to sediment produced from erosion. The spatial distribution of $\omega^*_{i,w/s}$ shows that the relative amount of water power available to produce and transport sediment increases from 36 to 653 (mean ± standard deviation = 254±149) from the headwaters to the catchment mouth (Fig. 6C). We interpret this factor of 18 change to reflect shifts from headwaters to outlet in dominant geomorphic processes. For example, on headwater slopes where less water is available and $\omega^*_{i,w/s}$ is lowest, we might expect that sediment transport is dominated by gravity-driven mass wasting and that weathering is dominated by physical rather than chemical processes. In contrast, on slopes near the catchment mouth, where $\omega^*_{i,w/s}$ is highest, we might expect that sediment transport is dominated by water-driven erosion (e.g., via sheetwash and channelized flow), and that weathering is dominated by chemical processes. This is broadly consistent with field observations: headwater slopes consist of steep, landslide-dominated bare bedrock, whereas slopes near the catchment outlet are gentler, more vegetated, and soil mantled, implying that chemical weathering is favored by longer residence times of water and sediment (Riebe et al., 2015).

Power for a given material can also be characterized at the scale of whole catchments. To do this, we sum Equation 3 over the entire contributing area, using Equation 5

$$\omega_{c,j} = g \sum_{i=1}^{i=N} \rho_{i,j} A_i \frac{\partial h_{i,j}}{\partial t} \frac{\left(z_i - z_o\right)}{L_i} \quad (5).$$

Here $\omega_{c,j}$ is the catchment-integrated source-area power for the material of interest *j*, or, more simply, "catchment power." It expresses the total power expended as the potential energy of material produced throughout the catchment is lost along flow paths to the outlet. For Inyo Creek, the total catchment power for water is 166 W m^{-1}, while the total catchment power for sediment is 0.122 W m^{-1}. The ratio of catchment power for water to sediment is 136. This ratio reflects the combined effects of the steep altitudinal increase in erosion rates, the more modest altitudinal increase in precipitation rates, and how these trends map onto the joint distribution of elevation and travel distance.

New theory and data from other landscapes are needed to interpret spatial variations in power across individual catchments and to understand why they vary from catchment to catchment. For example, we might expect to find a different spatial distribution of water-sediment power ratios, relative to Inyo Creek, in a catchment with a different hypsometry and width function. Likewise, the spatial distribution of source-area power would differ greatly in a catchment responding to accelerated base-level lowering, with

faster erosion rates near the outlet. More generally, we might expect the ratio of water to sediment catchment power to vary considerably from catchment to catchment across gradients in climate and tectonics. Understanding these variations could provide fresh insights into the geomorphic processes that shape landscapes.

Although our analysis of power at Inyo Creek focused on the production of water and sediment, it can be extended to any material that varies in production rate with altitude or varies in delivery to the outlet as a function of travel distance. For example, production rates of solutes, nutrients, contaminants, and even cosmogenic nuclides could be substituted for the production rate terms in Equations 2-5. Thus it should be possible to use the new frameworks of source-area and catchment power to model, and thus better understand, both the spatial distribution and catchment-integrated effects of geomorphic, geochemical, and ecosystem processes.

Our analysis of Inyo Creek shows how the power framework can be applied to natural landscapes using a DEM. However, factors, such as climate, topography, and tectonics, which might influence power and thus merit further investigation, are closely coupled together. This makes it difficult to isolate any single factor of interest in comparisons of power across catchments. Moreover, some catchments, such as Providence Creek, have peculiarities in shape and structure that dominate patterns of power (Fig. 5b) and thus might confound comparisons of one catchment to the next. To overcome the limitations of using DEMs from individual catchments, we developed an approach that generates synthetic catchments based on scaling relationships for catchment geometry and topography. With this approach we can systematically explore how variations in factors such as area, relief, and profile concavity influence the distribution of source-area and catchment power in landscapes. In the next section we show that our synthetic catchments capture the fundamental characteristics of the joint distribution of elevation and travel distance in landscapes and thus can be used to isolate and study the influence of the physical, chemical and biological factors that govern catchment processes.

4 Synthetic joint distributions of elevation and travel distance

Our objective in developing synthetic catchments is to generate realistic joint distributions of elevation and travel distance (e.g., that are comparable to those shown in Fig. 3). Equations 3-5 show that this should be sufficient to quantify distributions of source-area and catchment power. Hence there is no need for a spatially explicit representation of topography, because calculating source-area power does not require information about spatial position of channels or topographic factors such as hillslope gradient or curvature. Populating the joint distribution of elevation and travel distance only requires specifying the upper and lower boundaries at each travel distance and then distributing area across elevations in the space between the boundaries. Although theory is available to generate main-stem longitudinal profiles that could serve as a realistic lower boundary of the distribution, we are unaware of any theory for predicting ridge profiles and thus delineating a realistic upper boundary. Most importantly, to our knowledge, no theory is available for populating the elevation distribution for a given travel distance between the upper and lower

boundaries, without creating a spatially explicit synthetic DEM using a landscape evolution model (Coulthard, 2001; Willgoose, 2005; Tucker and Hancock, 2010).

As a starting point for overcoming these limitations, we adopt a statistical, empirical approach, using Inyo Creek as a prototype for a relatively simple, symmetrical low-order catchment. We start with the actual maximum and minimum elevations at each travel distance and use a statistical optimization procedure to find the best-fit distribution of elevations. We then develop expressions for the upper and lower boundaries at each travel distance and use the best-fit area-versus-elevation function to define a fully synthetic joint distribution of elevation and travel distance.

4.1 Area-versus-elevation at each travel distance

To find the best-fit relationship between area and elevation at each travel distance, we parsed the Inyo Creek catchment into forty-seven 100-m wide travel distance bins (Fig. 7A). Figure 7B shows distributions of area with elevation for seven representative travel distance bins. Inspection of figure 7B suggests that the area under the curves scales with local relief (i.e., the width across the base of the curve), and that the distributions are consistently right skewed, with more area at the lower elevations. When we sum area and relief across all bins, and plot the fractional area versus fractional relief for each bin, we find that the data roughly follow a 1:1 line (Fig. 7C). We obtain a similar result for a variety of bin spacings, which suggests that the area-elevation relationship is self similar: when the upper and lower boundaries are farther apart (i.e., when local relief is higher), the area contained within the travel distance bin increases in direct proportion to the difference in relief. This permits a collapse of the distributions of elevation for each travel distance bin, by normalizing elevation with local relief, and area by total area in the bin. Figure 7D shows the normalized hypsometry for travel distance bins spanning the entire Inyo Creek catchment. The broad consistency of the shapes of the normalized distributions suggests that a single functional form could represent the central tendency, spread and even the skew of the distribution of area with elevation for any travel distance across the catchment.

The beta distribution has a simple functional form that captures two key characteristics of the normalized area-elevation relationships: it is bounded by 0 and 1, and it can have right-skew depending on the values of its two shape factors, α and β. Thus a beta distribution is well suited to generating synthetic distributions of area as a function of elevation.

A generic form of the beta distribution is shown in Equation 6

$$f_\beta = x^{\alpha-1}\left(1-x\right)^{\beta-1} \quad (6).$$

Here f_β is the height of the beta distribution at point x, where x ranges from 0 to 1 and the sum of area under the curve is equal to 1.

To find the values of α and β that correspond to the best fit between the area-elevation data and the beta distribution across all travel distances at Inyo Creek, we first converted Equation 6 to Equation 7 for dimensional consistency.

$$f_{A(z,L)} = A_L \left(z^*\right)^{\alpha-1} \left(1-z^*\right)^{\beta-1} \quad (7).$$

Here, $f_{A(z,L)}$ is the height of the scaled beta distribution at elevation z in travel distance bin L, A_L is the area in the travel distance bin, and $z^* = \left(z - z_C\right) / \left(z_R - z_C\right)$ where z_C is the elevation of the channel, and z_R is the elevation of the ridge.

By applying Equation 7 to each travel distance bin, we can generate a synthetic joint distribution of elevation and travel distance. We then can calculate the misfit between the synthetic and actual joint distributions as the square root of the mean squared differences (RMSE) at each elevation and travel distance. To find the best-fit parameters, we used an optimization algorithm to search for the pair of shape factors that minimize the misfit. For Inyo Creek data, with 100 m travel distance bins, and 40 m elevation bins (Fig. 7), the best-fit α is 2.6 and best-fit β is 3.4. The objective function for this case is shown in Figure 8. The best-fit parameters yield a beta distribution that follows the trend in the normalized area distributions shown in Figure 7D.

To quantify the model performance, we use the Nash-Sutcliffe model efficiency statistic (*NS*) (Nash and Sutcliffe, 1970), which is calculated as

$$NS = 1 - \frac{\sum \left(f_{A-Model} - f_{A-Data}\right)^2}{\sum \left(f_{A-Mean} - f_{A-Data}\right)^2} \quad (8).$$

Here the subscript 'model' refers to the predictions of Equation 7, 'data' refers to the DEM, and 'mean' represents a uniform area density in each bin equal to the total area divided by the number of distance and elevation bins containing data. A model efficiency of 1 implies a perfect match between predictions and observations. An efficiency of 0 indicates that model predictions are only as accurate as simply using the mean of the observed data. Less than zero efficiency (NS < 0) implies that the observed mean is a better predictor than the model. In other words, the closer the model efficiency is to 1, the more accurate the model is. For this particular binning scheme (100 m distance and 40 m elevation bins), the Nash-Sutcliffe model efficiency statistic for Inyo Creek is 0.41, indicating good but not excellent agreement with the topographic data.

To explore the sensitivity of model performance to spatial resolution of the binning scheme, we repeated the optimization procedure described above for a range of travel distance and elevation bin sizes. As shown in Figure 9A, the NS values are generally higher for larger bin sizes (i.e. fewer bins), reaching a local maximum (NS > 0.7) for 400 m travel distance bins. Model efficiency approaches 1.0 (NS > 0.9) for a single distance bin, which is equivalent to fitting the whole catchment hypsometry with a single beta distribution curve.

These results reveal a tradeoff between model performance and spatial resolution. They also suggest that, to first order, Equation 7 can capture much of the structure of area as a function of relief at Inyo Creek. To the extent that we can think of Inyo Creek as a prototypical catchment, we can use Equation 7 to generate synthetic joint distributions of elevation and travel distance for other catchments, with different channel and ridge profiles.

The good fit between the modeled and observed joint distributions of elevation and travel distance at Inyo Creek arises in part because the actual profiles of the channel and ridge were used as envelopes on the area-elevation distributions. This ensures that the boundaries of the modeled joint distribution correspond to actual topographic data. To generate a fully-synthetic joint distribution of elevation and travel distance, an approach is needed that not only distributes area across elevations but also produces synthetic channel and ridge profiles that define the upper and lower boundaries of elevation as a function of travel distance.

4.2 Main-stem channel and ridge profiles

For any travel distance, the lowest elevation will be on the channel main-stem. Thus, the main-stem long profile is the lower boundary for the joint distribution of elevation and travel distance. Channel elevations (z_C) are commonly modeled as a power function of travel distance (x) along the main stem from the outlet to the upstream limit of fluvial processes (i.e., the distance to the "channel head", denoted x_{ch}). As elaborated in the appendix, here we derive an expression for channel elevation that extends all the way to the top of the catchment, at the point where the valley axis meets the drainage divide.

From the outlet to x_{ch}, the elevation of the channel can be written as:

$$z_C = k_C\left[\left(L_{\max}\right)^{1-\theta H} - \left(L_{\max} - x\right)^{1-\theta H}\right] \text{for } 0 \le x \le x_{ch} \quad \text{(9a).}$$

Here, L_{max} is the travel distance to the outlet from the furthest point in the catchment, θ and H are the exponents in Flint's Law and Hack's Law respectively, and k_C is a constant that lumps together θ, H and other factors, as shown in the appendix.

For the valley axis upstream of the channel head, from x_{ch} to L_{max}, the elevation profile can be written as follows (see appendix for derivation):

$$z_C = k_C\left[\left(L_{\max}\right)^{1-\theta H} - \left(L_{ch}\right)^{1-\theta H}\right] + S_h\left(x - x_{ch}\right) \qquad \text{for } x_{ch} < x \le L_{\max} \quad \text{(9b)}$$

Here, L_{ch} is the distance from the channel head to the outlet and S_h represents a uniform slope over the distance between L_{ch} and L_{max}.

The upper boundary of the joint distribution of elevation and travel distance is defined by the collection of points at the highest elevations in each travel distance bin. Unlike the channel profile, which defines the base of the joint distribution, the points at the upper boundary do not necessarily lie along a

442 contiguous path. Nevertheless, for simplicity we refer to these points as the ridge profile, and assume that
443 its elevation follows a simple power-law relationship with distance.

444 $$z_R = k_R x^P \tag{10}$$

445 Here k_R is an adjustable parameter and the exponent P depends on the parameters of the channel profile. As
446 elaborated in the appendix, we impose the constraints that the ridge profile intersects the main-stem
447 channel profile at the two end points, where $x = 0$ and $x = L_{max}$, in order to define the parameter P.

448 **4.3 Scaling between area and relief**

449 Equations 9 and 10 provide the values of z_C and z_R that are needed in Equation 7 to define the local
450 relief for any travel distance. However, before Equation 7 can be used to generate synthetic distributions of
451 elevation and travel distance, the area in each travel distance bin (A_L) must be defined. We do so using the
452 previously discussed self-similar relationship between area and local relief shown in Figure 7C, where the
453 fraction of the total area in a travel bin of interest is proportional to the local relief divided by the sum of
454 local relief over all travel distance bins. For Inyo Creek, this relationship holds for any choice of bin
455 spacing and it is expressed mathematically in Equation 11

456 $$\frac{A_L}{A_C} = \frac{A_L}{\sum_{L=1}^{N} A_L} = \frac{R_L}{\sum_{L=1}^{N} R_L} \tag{11}.$$

457 Here, N is the number of bins, A_C is the catchment area, which is equal to the sum of all A_L, and R_L is the
458 relief in the travel distance bin, which is equal to z_R-z_C. Following Hack's Law, the total area of the
459 catchment (A_C) can be treated as a power function of L_{max} (see appendix).

460 **4.4 Generating synthetic distributions of elevation and travel distance**

461 Equations 7, 9, 10 and 11 can be used to generate fully synthetic distributions of elevation and
462 travel distance that are coupled to fundamental scaling relationships of natural catchments (expressed in
463 Hack's and Flint's laws). Moreover, this permits us to tune parameter values to reproduce catchments of
464 specific sizes and shapes. For example, Figure 10 shows the synthetic joint distribution of elevation and
465 travel distance for a catchment with size and shape similar to Inyo Creek (see appendix for the list of model
466 parameters used to generate this plot). By projecting the joint distribution of elevation and travel distance
467 onto the two orthogonal axes, we obtain the hypsometric curve and width function for the synthetic
468 catchment (Fig. 10, panels B and C). Thus, although the hypsometry and width function cannot be used
469 alone or together to generate the joint distribution of elevation and travel distance, they can be derived from
470 it. Nash-Sutcliffe statistics calculated from a comparison of the fully synthetic (Fig. 10A) and true
471 distribution (Fig. 4D) vary with bin size as in the previous case using the actual channel and ridge profiles,

as shown in Figure 9. However, NS values for a given binning scheme are generally lower. This result suggests that the fully synthetic formulation is less efficient than the partly synthetic formulation of section 4.1 at explaining variance in the joint distribution of elevation and travel distance. This loss of efficiency arises due to error in fitting the upper and lower boundaries with the channel and ridge profile curves of Equations 9 and 10.

5. Discussion

5.1 Extending the model to other catchments

The fully synthetic formulation for the joint distribution of elevation and travel distance was calibrated using data from Inyo Creek, under the assumption that it is a prototypical catchment. But Inyo Creek is relatively small and steep. This raises the question of whether the synthetic formulation yields realistic results in other landscapes with lower relief or higher area.

Our other two study catchments, Providence Creek and Noyo River have lower relief and greater area, respectively (Fig. 1). Hence we can use them to gauge the performance of the synthetic formulation across a range of conditions. First we evaluated how well the beta distribution can be used as a predictor of the distribution of elevation at each travel distance. Results are shown in Figure 11, which displays normalized area-versus-elevation distributions for Providence Creek and Noyo River together with the best-fit beta distributions for each catchment (with travel distance and elevation binned at 1/20 of maximum values). The central tendency, spread, and skew of the best-fit beta distributions all appear to roughly follow the patterns exhibited in the data. However, the values of the best-fit shape parameters differ between these two catchments, as well as with Inyo Creek for this binning scheme. This suggest that the joint distribution of travel distance and elevation, as represented by these model parameters, may differ systematically between catchments.

The three catchments we analyzed vary across gradients in relief and drainage area (Fig. 1), but also in the degree of dissection and channel profile shape, which may in turn reflect differing lithologic, tectonic or climatic boundary conditions. For example, Providence Creek has a pronounced step in the channel profile, with greater local relief and area concentrated in the upper part of the catchment (Fig. 2). This step may arise due to feedbacks between weathering of biotite and topographic slope across the landscape (Wahrhaftig, 1965). As a result, the channel profile is not well-fit by a power equation or any other simple function. In contrast, the larger Noyo River catchment has a smooth, highly concave main-stem channel profile, and greater area at longer travel distances to the outlet due to a high degree of channel branching. The Noyo River main-stem channel profile may be influenced by aggradation due to sea-level rise, and is better represented in the fully synthetic model using an exponential equation instead of a power equation (see appendix).

Another second way to gauge model performance for various catchments is to compare predicted hypsometric curves and width functions using the projections of the modeled and measured joint distributions onto the elevation and travel distance axes, as we did in Fig. 10 for the fully synthetic Inyo Creek case. Figure 12 shows hypsometric curves and width functions for the three study catchments generated with the DEM data ('actual'), the partially-synthetic formulation using actual profiles and modeled area distributions (Eqns. 7 and 11), and the fully-synthetic formulation using modeled profiles. For Inyo Creek, both the partly and fully synthetic models provide good fits to the overall shape of the actual hypsometry and width function (Fig. 12a-b). In contrast, at Providence Creek, the partly synthetic model only captures the hypsometry and width function over portions of the distributions, and performs particularly poorly in the wide upper part of the catchment (Fig. 12c-d). Meanwhile, the fully synthetic model performs more poorly because the modeled channel profile fails to capture the step in the topography (Fig. 12 c-d). At Noyo River, despite its larger area, both the partly and fully synthetic models perform reasonably well over all elevations and travel distances. Together these results suggest that both the hypsometry and the width function of a wide range of catchments can be approximated to first order using the framework developed here, provided that variations in the channel profile can be modeled.

5.2 Future research opportunities

Our results suggest many potentially fruitful avenues for future research. First, joint distributions of travel distance and elevation, combined with knowledge of rates of precipitation, erosion or other material fluxes, can be used to understand how energy is created and dissipated across landscapes. The concept of source-area power provides a quantitative measure of the spatial distribution of processes that influence the supply of materials to the catchment outlet. For example, this framework can be used to understand how the size distribution of sediments passing through a catchment outlet is influenced by weathering conditions at source elevations (Sklar et al., 2016), and by particle breakdown in transport (Attal and Lave, 2009). Specifically, the initial particle size produced on hillslopes may vary systematically with local climate, vegetation, and erosion rate, factors that commonly vary with elevation within catchments (Riebe et al., 2015). In the absence of particle size reduction in transport, the size distribution of sediments delivered to the outlet would then reflect the distribution of source elevations, weighted by the local erosion rate. Yet particle wear is likely to be significant except in small catchments underlain by exceptionally durable rock. The overall extent of particle size reduction in transport will depend on the distribution of travel distances and the rates of energy dissipation along those transport paths. Thus the evolution of sediment sizes in catchments, from source areas to the catchment outlet, and the resulting size distribution passing through the outlet, depend on the factors that together determine source-area power.

Second, catchment power, the integral of source-area power for a given material over the entire catchment (equation 5), provides a metric for comparisons between catchments, and could be used to

quantify, and help explain, the variation in topography across gradients in climate, tectonics and lithology. For example, Reiners et al., 2003, found a strong correlation between spatial variation in erosion rate and precipitation in the Cascade Mountains of Washington, but no corresponding trend in conventional topographic indices such as local relief. Catchment power, calculated for water delivered by precipitation, for sediment produced by erosion, or as the ratio of water to sediment power, could provide a metric that captures how topography varies across gradients in precipitation and erosion. In this way, catchment power could help explain how topography mediates the linkage between climate and tectonics. Catchment power could also be used to compare numerical simulations of landscape evolution with real landscapes (Willgoose 1994; Willgoose et al., 2003), and contrast terrestrial catchments with catchments on Mars or Titan, where the topography reflects differing gravitational accelerations, fluids and rock properties (Mest et al., 2010; Burr et al., 2012).

A third set of research questions emerges from our approach to modeling synthetic joint distributions of elevation and transport distance. What explains the common tendency for positive skew in the distribution of area with elevation for a given travel distance? What do differences in the strength of this asymmetry from one catchment to another tell us about landscape-forming processes? Why are area and local relief within a travel distance bin linearly proportional, and does this relationship hold across a wider suite of catchments? Can the model of a fully synthetic catchment be used to represent landscapes across greater ranges of relief and drainage area than explored here?

Finally, the apparent success of our empirical model in capturing the bulk trends in the joint distribution of elevation and travel distance in our study catchments suggests that there may be value in developing a more comprehensive model, which accounts explicitly for the branching structure of the channel network. Such a model might have at its core a representation of the distribution of elevation and travel distance for a first-order catchment similar to our empirical model for Inyo Creek. The model would then represent larger catchments as combinations of multiple first-order headwater sub-catchments, and the hillslope facets that drain directly to higher-order channel segments. This raises the question of whether there is a characteristic distribution of elevation for a given travel distance in the facets draining higher-order valley slopes, and does it differ from the headwater sub-catchments in the same landscape? Variation in the topology of branching networks will shift the relative contributions of headwater sub-catchments and higher-order facets to the number of source-areas at a given elevation or travel distance. How sensitive are the distributions of source-area power to variations in network topology? Ultimately, such a model may help explain both the central tendency and variability in the joint distribution of elevation and travel distance, and provide a stronger theoretical foundation for understanding the three-dimensional structure of catchment topography.

6 Summary

Here we showed that the joint distribution of elevation and travel distance provide insight into the vertical and horizontal structure of catchments in mountain landscapes, which is not provided by the conventional metrics of catchment hypsometry and width function (Fig. 4). We then showed that the paired values of elevation and travel distance can be collapsed into a single index – the mean slope along the travel path – which varies both within and across catchments (Fig. 5). Mean slope can be combined with knowledge of the fluxes and density of materials produced at, or delivered to source areas, to define source-area power, and its integral catchment power, new metrics for quantifying spatial variations in hydrologic and geomorphic processes within and between catchments (Fig. 6). To enable modeling of processes influenced by source-area power, we developed an empirical statistical framework for defining the joint distribution of elevation and travel distance. We used the Inyo Creek catchment as a prototype, and found that the distribution of elevation between the main-stem channel and ridge profiles, for a given travel distance bin, is well-represented by a parameterization of the beta distribution. To define a fully synthetic catchment, we derived power-law and exponential expressions for the channel and ridge profiles, which when combined with the model for elevation distribution, can produce realistic hypsometric curves and width functions. Key questions emerging from this work include: how do patterns of source-area and catchment power vary across spatial gradients in climate, tectonics and lithology? What explains the characteristic skew of elevation distributions for a given travel distance? And how do the patterns in the distributions of source-area and catchment power arise from the branching properties of networks and the relief structure of landscapes?

Appendix A: Derivation of channel and ridge profile equations

A.1 Main-stem channel power-law profile

To create an expression for the longitudinal profile of the main-stem channel, we coupled the widely observed power-law scaling between slope (S) and drainage area (A)

$$S = k_s A^{-\theta} \tag{A1}$$

and the likewise common power-law scaling of main-stem distance (L) and area

$$A = k_A L^H \tag{A2}.$$

In Equation A1, known as Flint's law, k_s and θ are empirical coefficients (where θ is referred to as profile concavity). In Equation A2, a version of Hack's law, L is a local distance downstream from the catchment divide along the main-stem valley axis, and k_A and H are empirical coefficients (with H the reciprocal of the

Hack exponent). Hack's law can also be written in terms of the local travel distance upstream of the catchment outlet, x,

$$A = k_A \left(L_{\max} - x \right)^H \tag{A3}$$

where L_{max} is the value of L at the outlet (i.e., $x = L_{max} - L$).

Combining equations A1 and A3 we obtain an expression for mainstem channel slope, S_C, as a function of distance upstream x

$$S_c = \frac{\partial z_c}{\partial x} = k_s k_A^{-\theta} \left(L_{\max} - x \right)^{-\theta H} \tag{A4}$$

where z_c is the elevation of the mainstem channel.

Integrating equation A4 provides an expression for the mainstem longitudinal profile

$$z_C = k_C \left[\left(L_{\max} \right)^{1-\theta H} - \left(L_{\max} - x \right)^{1-\theta H} \right] \tag{A5a}$$

where

$$k_C = \frac{k_s k_A^{-\theta}}{1 - \theta H} \tag{A5b}$$

Equation A5 is valid for the fluvial portion of the channel network. However, at small drainage areas, and the fluvial slope-area scaling (Eqn. A1) does not apply. Typically, slope changes much less rapidly as drainage changes in this part of the landscape. For simplicity we assume that slope is constant above a point on the longitudinal profile that we refer to as the channel head.

We define a distance L_{ch} which is the travel distance from where the valley axis meets the drainage divide down to the channel head; subscript *ch* indicates channel head. The elevation at the channel head, where $x = x_{ch} = (L_{\max} - L_{ch})$ is

$$z_C = k_C \left[\left(L_{\max} \right)^{1-\theta H} - \left(L_{ch} \right)^{1-\theta H} \right] \tag{A6}.$$

The drainage area at the channel head A_{ch} is

$$A_{ch} = k_A L_{ch}^H \tag{A7}$$

and the constant gradient above this point S_h is

$$S_h = k_s A_{ch}^{-\theta} = \frac{k_s}{k_A^{\theta}} L_{ch}^{-\theta H} \tag{A8}$$

Thus the elevation of the long profile, from bottom to top can be written as follows:

$$z_C = k_C\left[\left(L_{\max}\right)^{1-\theta H} - \left(L_{\max} - x\right)^{1-\theta H}\right] \text{for } 0 \le x \le x_{ch} \quad \text{(A9)}$$

$$z_C = k_C\left[\left(L_{\max}\right)^{1-\theta H} - \left(L_{ch}\right)^{1-\theta H}\right] + S_h\left(x - x_{ch}\right) \quad \text{for } x_{ch} < x \le L_{\max} \quad \text{(A10)}$$

The highest point along the mainstem profile, z_{C_max} is

$$z_{C\_max} = k_C\left[\left(L_{\max}\right)^{1-\theta H} - \left(L_{ch}\right)^{1-\theta H}\right] + S_h L_{ch} \quad \text{(A11)}$$

A.2 Ridge power-law profile

To define the ridge long profile, we assume a simple power-law relation between elevation and distance,

$$z_R = k_R x^P \quad \text{(A12)}$$

where k_R is an adjustable parameter and the exponent P depends on the parameters of the channel profile. To specify P we impose the constraints that the ridge profile must intersect the mainstem channel profile at the two end points, where $x = 0$ and $x = L_{max}$, the lowest and highest points in the landscape.

With the constraints that the elevation of the ridge z_r and the channel z_c match where $x = 0$ and $x = L_{max}$, we can solve for the exponent P as follows:

$$P = \frac{\log\left(z_{c\_\max} / k_R\right)}{\log\left(L_{\max}\right)} \quad \text{(A13)}$$

Thus, the ridge network and the channel network are pinned together at the two end points.

A.3 Inyo Creek power-law profile parameters

The combined model for the ridge and channel profiles has 6 parameters; all other values are calculated from the equations above. For the Inyo Creek channel and ridge profiles extracted from the distributions of elevation for travel distances binned in 50 meter increments, Table A1 lists one possible set of values that adequately reproduce the observed profile. These values were tuned to satisfy the following constraints: L_{max} = 4700 m, the range of travel distances of Inyo rounded to nearest 50 m; drainage area at outlet = 3.4 km^2; maximum elevation above outlet of 1890 m

652 **A.4 Main-stem channel exponential profile**

653 Exponential profiles have been used by many, including Hack (cites). Simply state elevation of the
654 channel as increasing exponentially with distance upstream of the outlet

655 $$z_c = k_e e^{\lambda x} \tag{A14}$$

656 where k_e and lambda are empirical coefficients. As with the power profile, this is only valid between the
657 outlet and the channel head, where for simplicity we assume the slope becomes uniform. For the
658 exponential profile (equation A14), the channel slope

659 $$S_c = \frac{\partial z}{\partial x} = \lambda k_e e^{\lambda x} \tag{A15}$$

660 grows too slowly with increasing distance upstream of the channel head to represent the steep headwater
661 valley axis slope, so we define Sh-exp as an independent empirical model constant, with the constraint is
662 that it must be greater than the slope of the exponential profile at the channel head

663 $$S_{h\_\exp} > S_{c\_\max} = \lambda k_e e^{\lambda(L_{\max} - L_{ch})} \tag{A16}.$$

664 The full channel profile expression becomes

665 $$z_c = k_e e^{\lambda x} \qquad \text{for } 0 \le x \le x_{ch} \tag{A17a}$$

666 $$z_c = k_e e^{\lambda x_{ch}} + S_{h\_\exp}\left(x - x_{ch}\right) \qquad \text{for } x_{ch} < x \le L_{\max} \tag{A17b}$$

667 and the highest point along the mainstem profile, Z_{C_max} is

668 $$z_{c\_\max} = k_e e^{\lambda x_{ch}} + S_{h\_\exp} L_{ch} \tag{A18}.$$

669 **A.5 Ridge exponential profile**

670 To define the ridge long profile, for symmetry with the channel profile we assume an exponential
671 relation between elevation and distance,

672 $$z_R = k_{\mathrm{Re}} e^{\gamma x} \tag{A19}$$

673 Where the coefficient k_{Re} is an adjustable parameter, and the exponent γ depends on the parameters of the
674 channel profile. As with the power law profile derivation, to specify γ we impose the constraints that the
675 ridge profile must intersect the mainstem channel profile at the two end points, where $x = 0$ and $x = L_{max}$,
676 the lowest and highest points in the landscape.

With the constraints that the elevation of the ridge z_r and the channel z_c match where $x = L_{max}$, we can solve for the exponent γ

$$\gamma = \frac{\ln\left(z_{c\_\max} / k_{\mathrm{Re}}\right)}{L_{\max}} \tag{A20}$$

The ridge network and the channel network are pinned together at these two end points.

A.6 Inyo Creek exponential profile parameters

The combined model for the two exponential profiles has five parameters; all other values are calculated from the equations above. Table A2 lists one possible best fit (by eye) set of values for the Noyo River channel and ridge profiles extracted from the distributions of elevation for travel distances binned in 250 meter increments. These values were tuned to satisfy the following constraints: L_{max} = 20,750 m, the range of travel distances of Inyo rounded to nearest 50 m; maximum elevation above outlet = 620 m (along mainstem profile).

Data Availability

The DEMs used in this paper can be obtained upon request from the corresponding author.

Acknowledgments

We thank Sarah Konrad and Catherine Noll for contributing to preliminary DEM analysis, Colin Stark and Scott Peckham for thoughtful discussions, and two anonymous reviewers for helpful comments on an earlier draft. Funding was provided by the Doris and David Dawdy Fund for Hydrologic Research, and National Science Foundation Grants EAR 1325033 and 1239521.

References

Algeo, T. J., and Seslavinsky, K. B.: Reconstructing eustatic and epeirogenic trends from Paleozoic continental flooding records. In Sequence Stratigraphy and Depositional Response to Eustatic, Tectonic and Climatic Forcing (pp. 209-246). Springer Netherlands, 1995.

Attal, M., and Lavé, J.: Changes of bedload characteristics along the Marsyandi River (central Nepal): Implications for understanding hillslope sediment supply, sediment load evolution along fluvial networks, and denudation in active orogenic belts. Geological Society of America Special Papers, 398, 143-171, 2006.

Bales, R. C., Hopmans, J. W., O'Geen, A. T., Meadows, M., Hartsough, P. C., Kirchner, P., Hunsaker, C. T. and Beaudette, D.,: Soil moisture response to snowmelt and rainfall in a Sierra Nevada mixed-conifer forest.Vadose Zone Journal, 10(3), pp.786-799, 2011.

Brocklehurst, S. H., and Whipple, K. X.: Glacial erosion and relief production in the Eastern Sierra Nevada, California. Geomorphology, 42(1), 1-24, 2002.

Brocklehurst, S. H., and Whipple, K. X.: Hypsometry of glaciated landscapes. Earth Surface Processes and Landforms, 29(7), 907-926, 2004.

Brozović, N., Burbank, D. W., and Meigs, A. J.: Climatic limits on landscape development in the northwestern Himalaya. Science, 276(5312), 571-574, 1997.

Burbank, D. W., Blythe, A. E., Putkonen, J., Pratt-Sitaula, B., Gabet, E., Oskin, M., Barros, A., and Ojha, T. P.: Decoupling of erosion and precipitation in the Himalayas. Nature, 426(6967), 652-655, 2003.

Burns, J. W.: Some effects of logging and associated road construction on northern California streams. Transactions of the American Fisheries Society,101(1), 1-17, 1972.

Burr, D. M., Perron, J. T., Lamb, M. P., Irwin, R. P., Howard, A. D., Collins, G. C., Sklar, L.S., Moore, J.M., Adamkovics, M., Baker, V.R., Drummond, S.A., and Black B.A.: Fluvial features on Titan: Insights from morphology and modeling, Geological Society of America Bulletin, doi: 10.1130/B30612.2, 2012.

Coulthard, T. J.: Landscape evolution models: a software review. Hydrological processes, 15(1), 165-173, 2001.

Dai, J. J., Lorenzato, S., and Rocke, D. M.: A knowledge-based model of watershed assessment for sediment. Environmental Modelling and Software,19(4), 423-433, 2004.

Gaillardet, J., Dupré, B., and Allègre, C. J.: Geochemistry of large river suspended sediments: silicate weathering or recycling tracer?. Geochimica et Cosmochimica Acta, 63(23), 4037-4051, 1999.

Goulden, M. L., and Bales, R. C.: Mountain runoff vulnerability to increased evapotranspiration with vegetation expansion. Proceedings of the National Academy of Sciences, 111(39), 14071-14075, 2014.

Gupta, V. K., and Mesa, O. J.: Runoff generation and hydrologic response via channel network geomorphology—Recent progress and open problems. Journal of hydrology, 102(1), 3-28, 1988.

Gupta, V. K., and Waymire, E. D.: Statistical self‐similarity in river networks parameterized by elevation. Water Resources Research, 25(3), 463-476, 1989.

Hahm, W. J., Riebe, C. S., Lukens, C. E., and Araki, S.: Bedrock composition regulates mountain ecosystems and landscape evolution. Proceedings of the National Academy of Sciences, 111(9), 3338-3343, 2014.

Holbrook, W., Riebe, C. S., Elwaseif, M., Hayes, J. L., Basler‐Reeder, K., Harry, D. L., Malazian, A., Dosseto, A., Hartsough, P. C., and Hopmans, J. W.: Geophysical constraints on deep weathering and water storage potential in the Southern Sierra Critical Zone Observatory. Earth Surface Processes and Landforms, 39(3), 366-380, 2014.

Hunsaker, C. T., and Neary, D. G.: Sediment loads and erosion in forest headwater streams of the Sierra Nevada, California. In Proceedings of a workshop for the International Association of Hydrological Sciences, General Assembly in Melbourne. Revisiting Experimental Catchment Studies in Forest Hydrology. Wallingford, United Kingdom (pp. 195-204), 2012.

Hunsaker, C. T., Whitaker, T. W., and Bales, R. C.: Snowmelt runoff and water yield along elevation and temperature gradients in California's Southern Sierra Nevada, Journal of the American Water Resources Association (JAWRA) 48(4): 667-678. DOI: 10.1111/j.1752-1688.2012.00641, 2012.

Jin, L., Ravella, R., Ketchum, B., Bierman, P. R., Heaney, P., White, T., and Brantley, S. L.: Mineral weathering and elemental transport during hillslope evolution at the Susquehanna/Shale Hills Critical Zone Observatory, Geochimica et Cosmochimica Acta, 74(13), 3669-3691, 2010.

Lague, D.: The stream power river incision model: evidence, theory and beyond, Earth Surface Processes and Landforms 39.1 (2014): 38-61, 2014.

Lashermes, B., and Foufoula‐Georgiou, E.: Area and width functions of river networks: New results on multifractal properties, Water resources research, 43(9), 2007.

Leithold, E. L., Blair, N. E., and Perkey, D. W.: Geomorphologic controls on the age of particulate organic carbon from small mountainous and upland rivers. Global Biogeochemical Cycles, 20(3), 2006.

Lifton, N. A., and Chase, C. G.: Tectonic, climatic and lithologic influences on landscape fractal dimension and hypsometry: implications for landscape evolution in the San Gabriel Mountains, California.Geomorphology, 5(1), 77-114, 1992.

Lisle, T. E.: Effects of aggradation and degradation on riffle‐pool morphology in natural gravel channels, northwestern California. Water Resources Research, 18(6), 1643-1651, 1982.

763 Lomolino, M. A. R. K.: Elevation gradients of species‐density: historical and prospective views. Global
764 Ecology and Biogeography, 10(1), 3-13, 2001.
765 Marshall, J. A., and Sklar, L. S.: Mining soil databases for landscape‐scale patterns in the abundance and
766 size distribution of hillslope rock fragments, Earth Surface Processes and Landforms, 37(3), 287-
767 300, 2012.
768 Mest, S. C., Crown, D. A., and Harbert, W.: Watershed modeling in the Tyrrhena Terra region of
769 Mars, *Journal of Geophysical Research: Planets*,*115*(E9), 2010.
770 Minder, J. R., Durran, D. R., and Roe, G. H.: Mesoscale controls on the mountainside snow line. Journal of
771 the Atmospheric Sciences, 68(9), 2107-2127, 2011.
772 Moussa, R.: What controls the width function shape, and can it be used for channel network comparison
773 and regionalization?. Water Resources Research, 44(8), 2008.
774 Nash, J., and Sutcliffe, J. V.: River flow forecasting through conceptual models part I—A discussion of
775 principles. Journal of hydrology, 10(3), 282-290, 1970.
776 PRISM Climate Group, Oregon State University, http://prism.oregonstate.edu, 2014.
777 Raich, J. W., Russell, A. E., and Vitousek, P. M.: Primary productivity and ecosystem development along
778 an elevational gradient on Mauna Loa, Hawai'i. Ecology, 78(3), 707-721, 1997.
779 Reiners, P. W., Ehlers, T. A., Mitchell, S. G., and Montgomery, D. R.: Coupled spatial variations in
780 precipitation and long-term erosion rates across the Washington Cascades. Nature, 426(6967),
781 645-647, 2003.
782 Richey, J. E., Mertes, L. A., Dunne, T., Victoria, R. L., Forsberg, B. R., Tancredi, A. C., and Oliveira, E.:
783 Sources and routing of the Amazon River flood wave. Global biogeochemical cycles, 3(3), 191-
784 204, 1989.
785 Riebe, C. S., Kirchner, J. W., and Finkel, R. C.: Erosional and climatic effects on long-term chemical
786 weathering rates in granitic landscapes spanning diverse climate regimes. Earth and Planetary
787 Science Letters,224(3), 547-562, 2004.
788 Reibe, C. S., Sklar, L. S. Lukens, C. E. and Shuster, D. L.: Climate and topography control the size of
789 sediment produced on mountain slopes, Proceedings of the National Academy of Sciences, doi:
790 10.1073/pnas.1503567112, 2015.
791 Rigon, R., Rinaldo, A., and Rodriguez‐Iturbe, I.: On landscape self‐organization. Journal of Geophysical
792 Research: Solid Earth (1978–2012),99(B6), 11971-11993, 1994.
793 Rigon, R., Bancheri, M., Formetta, G., and de Lavenne, A.: The geomorphological unit hydrograph from a
794 historical‐critical perspective. Earth Surface Processes and Landforms, 2015.
795 Rinaldo, A., Vogel, G. K., Rigon, R., and Rodriguez‐Iturbe, I.: Can one gauge the shape of a basin? Water
796 Resources Research, 31(4), 1119-1127, 1995.
797 Rodríguez-Iturbe, I., Rinaldo, A., Rigon, R., Bras, R. L., Marani, A., and Ijjász-Vásquez, E.: Energy
798 dissipation, runoff production, and the three-dimensional structure of river basins. Water
799 Resources Research, 28(4), 1095-1103, 1992.

Roe, G. H.: Orographic precipitation. Annu. Rev. Earth Planet. Sci.,33, 645-671, 2005.

Sklar, L. S., Dietrich, W. E., Foufoula‐Georgiou, E., Lashermes, B., and Bellugi, D.: Do gravel bed river size distributions record channel network structure?.Water Resources Research, 42(6), 2006.

Sklar, L. S., Riebe, C. S., Marshall, J. A., Genetti, J., Leclere, S., Lukens, C. E. and Merces, V.: The problem of predicting the particle size distribution of sediment supplied by hillslopes to rivers, Geomorphology, doi:10.1016/j.geomorph.2016.05.005, 2016.

Stock, G. M., Ehlers, T. A., and Farley, K. A.: Where does sediment come from? Quantifying catchment erosion with detrital apatite (U-Th)/He thermochronometry. Geology, 34(9), 725-728, 2006.

Strahler, A. N.: Hypsometric (area-altitude) analysis of erosional topography, Geological Society of America Bulletin, 63(11), 1117-1142, 1952.

Taylor, B. R., and Chauvet, E. E.: Relative influence of shredders and fungi on leaf litter decomposition along a river altitudinal gradient, Hydrobiologia, 721(1), 239-250, 2014.

Tarboton, D. G.: A new method for the determination of flow directions and upslope areas in grid digital elevation models. Water resources research, 33(2), 309-319, 1997.

Tucker, G. E., and Hancock, G. R.: Modelling landscape evolution, Earth Surface Processes and Landforms, 35(1), 28-50, 2010.

Wahrhaftig, C.: Stepped topography of the southern Sierra Nevada, California. Geological Society of America Bulletin, 76(10), 1165-1190, 1965.

White, A. F., and Blum, A. E.: Effects of climate on chemical weathering in watersheds. Geochimica et Cosmochimica Acta, 59(9), 1729-1747, 1995.

Willgoose, G.: A statistic for testing the elevation characteristics of landscape simulation models. *Journal of Geophysical Research: Solid Earth*,*99*(B7), 13987-13996, 1994.

Willgoose, G.: Mathematical modeling of whole landscape evolution. Annu. Rev. Earth Planet. Sci., 33, 443-459, 2005.

Willgoose, G. R., Hancock, G. R., and Kuczera, G.: A framework for the quantitative testing of landform evolution models. *Prediction in Geomorphology*, 195-216, 2003.

828 **Figure captions**

829 **Figure 1. Study site locations and comparison of channel and ridge profiles.** Left: Location map of
830 study catchments in California, USA. Right: Elevation profiles of the lowest point at each travel distance
831 (i.e., the mainstem channel) and the highest point at each travel distance (referred to here as the ridge
832 profile). The longest and shortest travel distances in each catchment re the points where the two profiles
833 meet. The channel and ridge profiles enclose all paired values of elevation and travel distance for each
834 catchment. Differences in catchment relief and size across the sites produce distinct populations of paired
835 values. The ratio of elevation to travel distance is the mean slope along a path from the source to the
836 catchment outlet. Thus the catchments also harbor distinct populations of mean slope.

837 **Figure 2. Spatial distributions of elevation and travel distance.** Maps showing the spatial distribution of
838 elevation and travel distributions across the Inyo Creek (A), Providence Creek (B), and Noyo River (C)
839 study catchments. Black lines are elevation contours, with hillshade in background for emphasis. Color
840 shade shows scaled values of travel distance (normalized by the maximum value in the catchment). Note
841 variation in scale and compass orientation from one watershed to the next. Elevation contour spacing is 50
842 m in (C) and (B), and 200 m in (C).

843 **Figure 3. Hypsometry and width functions.** Normalized frequency distributions of elevation (a) and
844 travel distance to the outlet (b). Frequencies are normalized so that the area under the curve is equal to 1 in
845 each case. Binning increment is 1/47 of maximum value (Table 1).

846 **Figure 4. Joint distributions of elevation and travel distance.** Distribution of source area elevations and
847 travel distances from 10 m DEMs of catchments drained by (a) Inyo Creek, (b) Providence Creek, and (c)
848 the Noyo River. Bivariate frequency distributions of elevation and travel distance for each catchment (d-f)
849 show relative density (color bar in (d); data binning as in Figure 2.

850 **Figure 5. Distribution of mean slope across catchments.** Histograms (insets, A-C) of mean slope along
851 travel path from source to outlet (ratio of source area elevation to travel distance), with colors highlighting
852 bins of relatively low, medium and high values. Bins of common mean slope form linear bands on plots of
853 elevation versus travel distance (A-C). Maps of catchments (D-F) show spatial distribution of source areas
854 sharing similar mean slope for highlighted values.

855 **Figure 6. Spatial distribution of source-area power for water and sediment.** Histograms (left) of
856 source-area power calculated using equation 3 for the Inyo Creek catchment for water delivered by
857 precipitation (A), and sediment produced by erosion (B). Panel (C) shows dimensionless ratio of source-
858 area water power to sediment production rate (eqn. 4); colors highlight bins of relatively low, medium and
859 high values. Maps (right) show spatial distribution of highlighted values. Note the sharp increase in water
860 power per sediment flux from upper to lower parts of the catchment.

861 **Figure 7. Elevation distributions for different travel distances at Inyo Creek.** (A) Elevation data points
862 for Inyo Creek catchment parsed into forty-seven 100-m wide travel distance bins. (B) Distributions of

863 elevation for seven representative travel distance bins; colors correspond to shaded bins in panel A, mean
864 travel distance indicated for each curve. (C) Fraction of total area in each travel distance bin as a function
865 of fraction of total relief in each bin, roughly follows 1:1 line, colored symbols indicate representative bins
866 in panels A and B. (D) Collapse of elevation distributions for each travel distance bin, with elevation
867 normalized by relief within bin and area by total area within bin. Best-fit beta distribution captures typical
868 shape of hypsometry for a given travel distance.

869 **Figure 8. Objective function for best-fit beta distribution shape parameters.** Contour plot of root mean
870 sum of squared error (RMSE) between actual and predicted area density of elevation for a given travel
871 distance for paired values of beta distribution shape parameters. Minimum RMSE at $\alpha = 2.6$ and
872 $\beta = 3.4$ as indicated by diamond. In this example, travel distance and elevation bin sizes equal 100 m and
873 40 m respectively.

874 **Figure 9. Model performance**. Variation in Nash-Sutcliff model efficiency statistic (Eqn. 8) with size of
875 travel distance and elevation bins, for modeled joint distributions of elevation and travel distance for Inyo
876 Creek, using actual profiles (solid lines) and modeled profiles (dashed lines). Nash-Sutcliff value of 1.0
877 indicates perfect agreement between modeled and actual distribution of area; value of 0 indicates model
878 performance no better than uniform distribution of mean area density. A trade-off between model
879 efficiency and spatial resolution is revealed by trend toward higher Nash-Sutcliff values for larger bin sizes.

880 **Figure 10. Fully synthetic joint distribution of elevation and travel distance for catchment the size of**
881 **Inyo Creek**. In (A) channel and ridge profiles are defined by equations 9 and 10, area density (color bar)
882 given by equations 7 and 11. Side panels show area density projected on distance axis to create width
883 function (B) and projected on elevation axis to create hypsometric curve (C).

884 **Figure 11. Normalized Distribution of elevation by travel distance bin for other catchments**. Travel
885 distance and elevation bin sizes = 1/20 of maximum values Thin lines show elevation distributions,
886 normalized by local relief, for each travel distance bin. Thick colored curves show best-fit beta
887 distributions, with shape parameter values indicated. Normalized elevation distributions are more skewed
888 for Noyo River, reflecting larger drainage area and greater degree of landscape dissection.

889 **Figure 12. Comparison of actual with modeled hypsometric curves and width functions for three**
890 **study catchments.** In each panel, thick colored curves show data from catchment DEM, while thick and
891 dashed black lines show model predictions using actual and modeled channel and ridge profiles
892 respectively. Also shown in left panels are hypsometric curves predicted using uniform area distribution,
893 for the case when Nash-Sutcliff model efficiency statistic = 0; for this case, predicted width function
894 matches actual. Values in parenthesis indicate RMSE calculated by comparing model curves with DEM.

895

Table 1. Study site characteristics

	Inyo Creek	Providence Creek	Noyo River
Drainage Area (km^2)	3.4	8.1	144
Relief (m)	1,895	1,117	893
Max Travel Distance (m)	4,660	7,940	20,790
Mean Slope to outlet	0.33	0.14	0.021
Elevation of outlet (masl)	2053	998	84
Outlet UTM North	392369.717	300456.028	364182.531
Outlet UTM East	4049943.32	4101509.08	450994.25

Table A1. Inyo Creek power-law profile model parameters

Parameter	Value
θ	0.31
H	1.75
k_s	25
k_A	1.28
L_{ch}	600 m
K_R	0.6

Table A2. Noyo River exponential profile model parameters

Parameter	Value
λ	1.8 x10^{-4} m^{-1}
S_{h_exp}	0.16
k_e	6.7 m
L_{ch}	2000 m
K_{Re}	195 m

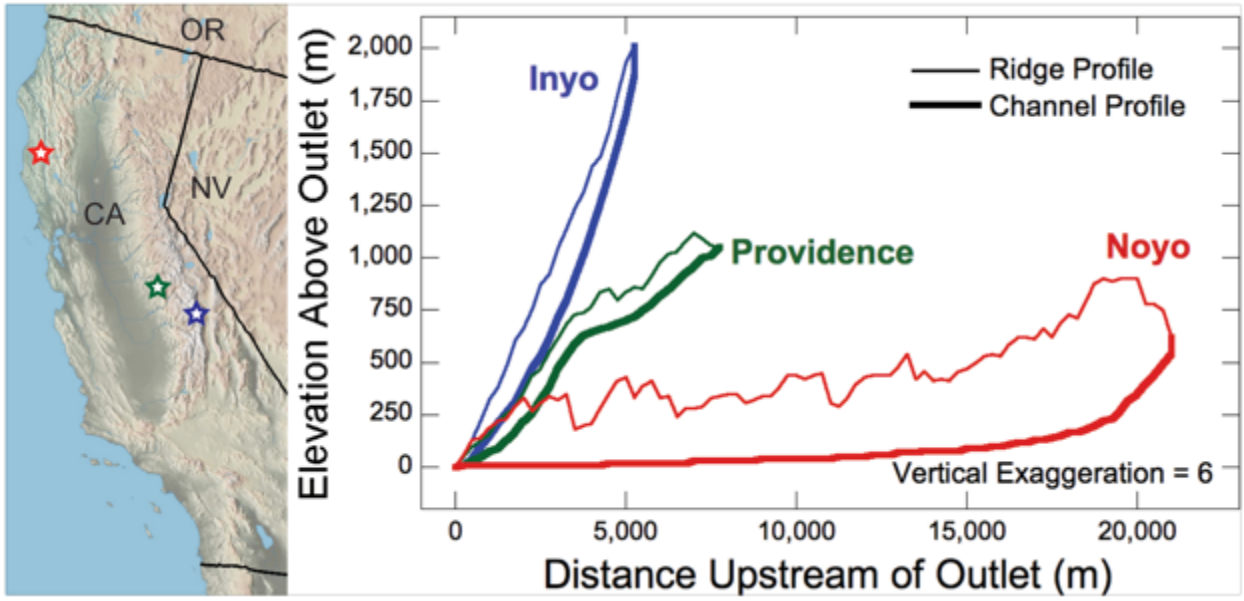

Figure 1. Study site locations and comparison of channel and ridge profiles. Left: Location map of study catchments in California, USA. Right: Elevation profiles of the lowest point at each travel distance (i.e., the mainstem channel) and the highest point at each travel distance (referred to here as the ridge profile). The longest and shortest travel distances in each catchment are the points where the two profiles meet. The channel and ridge profiles enclose all paired values of elevation and travel distance for each catchment. Differences in catchment relief and size across the sites produce distinct populations of paired values. The ratio of elevation to travel distance is the mean slope along a path from the source to the catchment outlet. Thus the catchments also harbor distinct populations of mean slope.

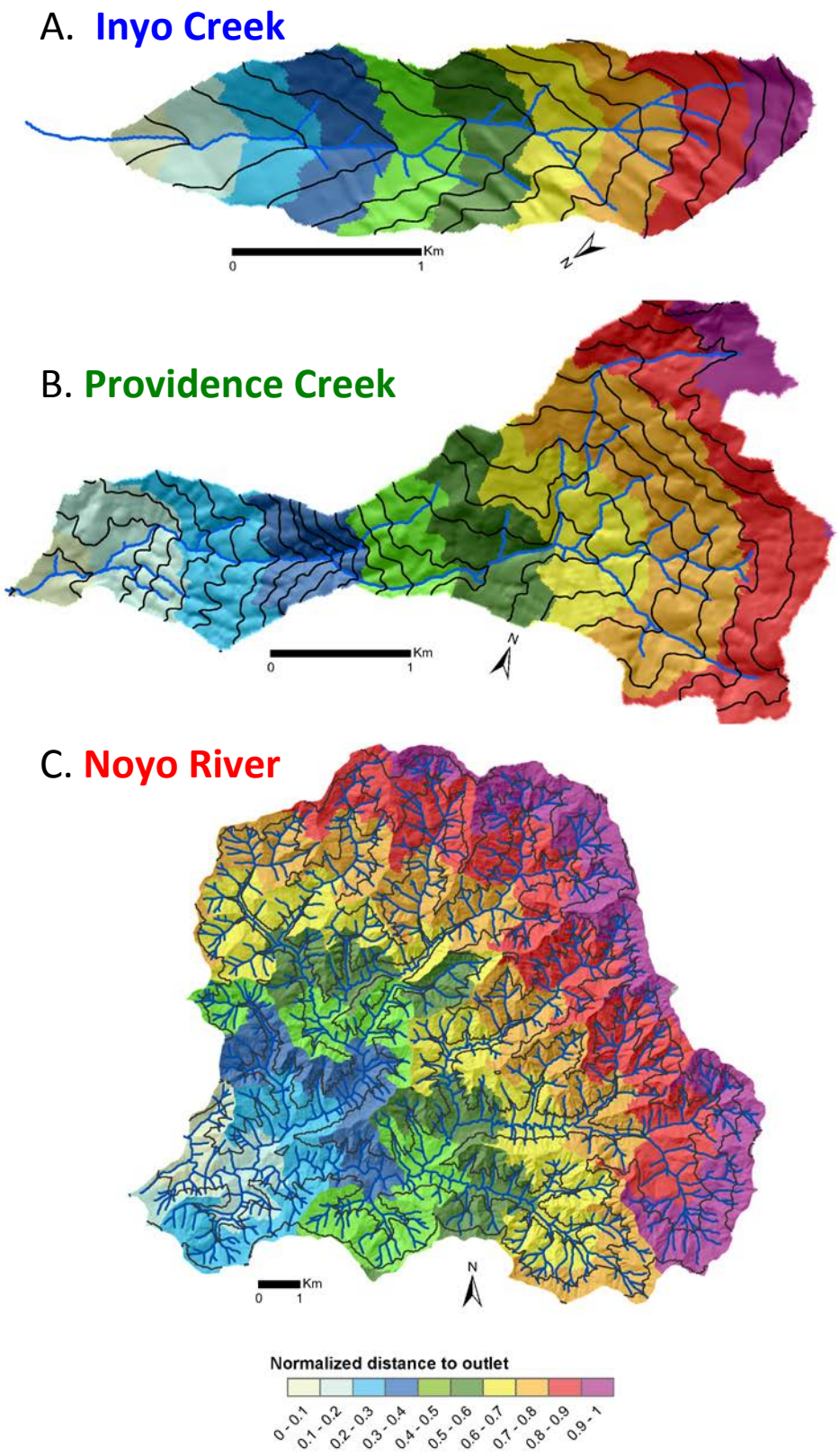

Figure 2. Spatial distributions of elevation and travel distance. Maps showing the spatial distribution of elevation and travel distributions across the Inyo Creek (A), Providence Creek (B), and Noyo River (C) study catchments. Black lines are elevation contours, with hillshade in background for emphasis. Color shade shows scaled values of travel distance (normalized by the maximum value in the catchment). Note variation in scale and compass orientation from one watershed to the next. Elevation contour spacing is 50 m in (C) and (B), and 200 m in (C).

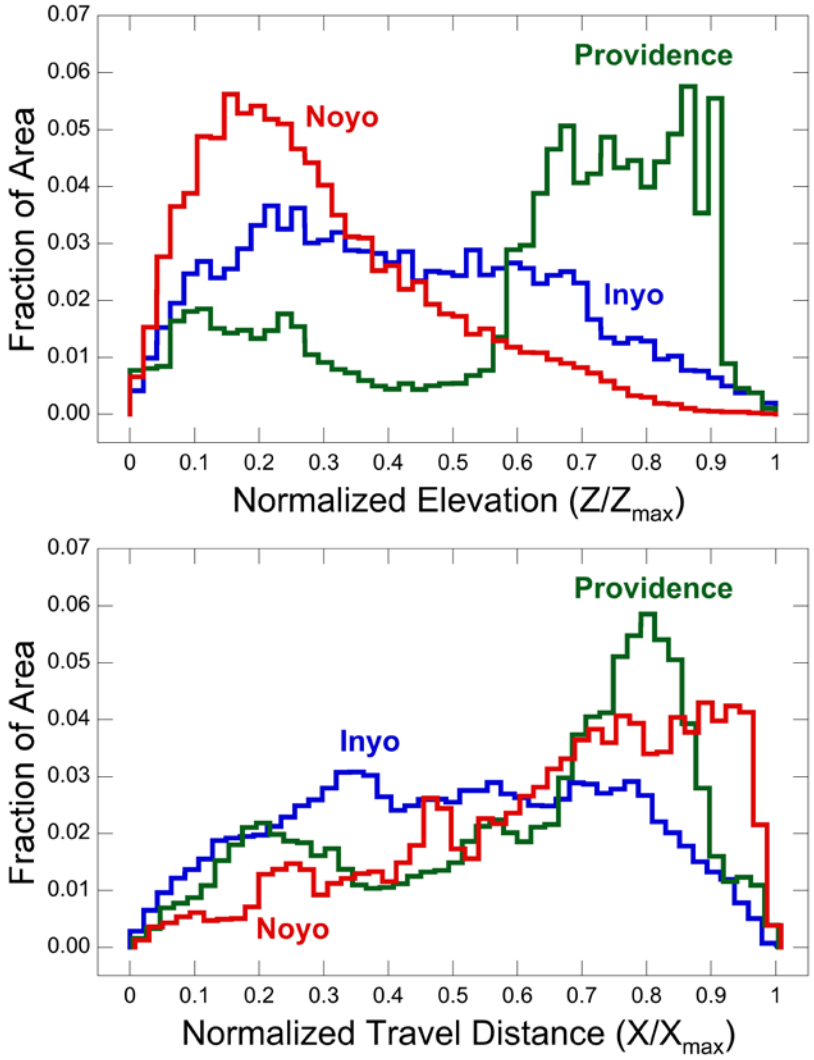

Figure 3. Hypsometry and width functions. Normalized frequency distributions of elevation (a) and travel distance to the outlet (b). Frequencies are normalized so that the area under the curve is equal to 1 in each case. Binning increment is 1/47 of maximum value (Table 1).

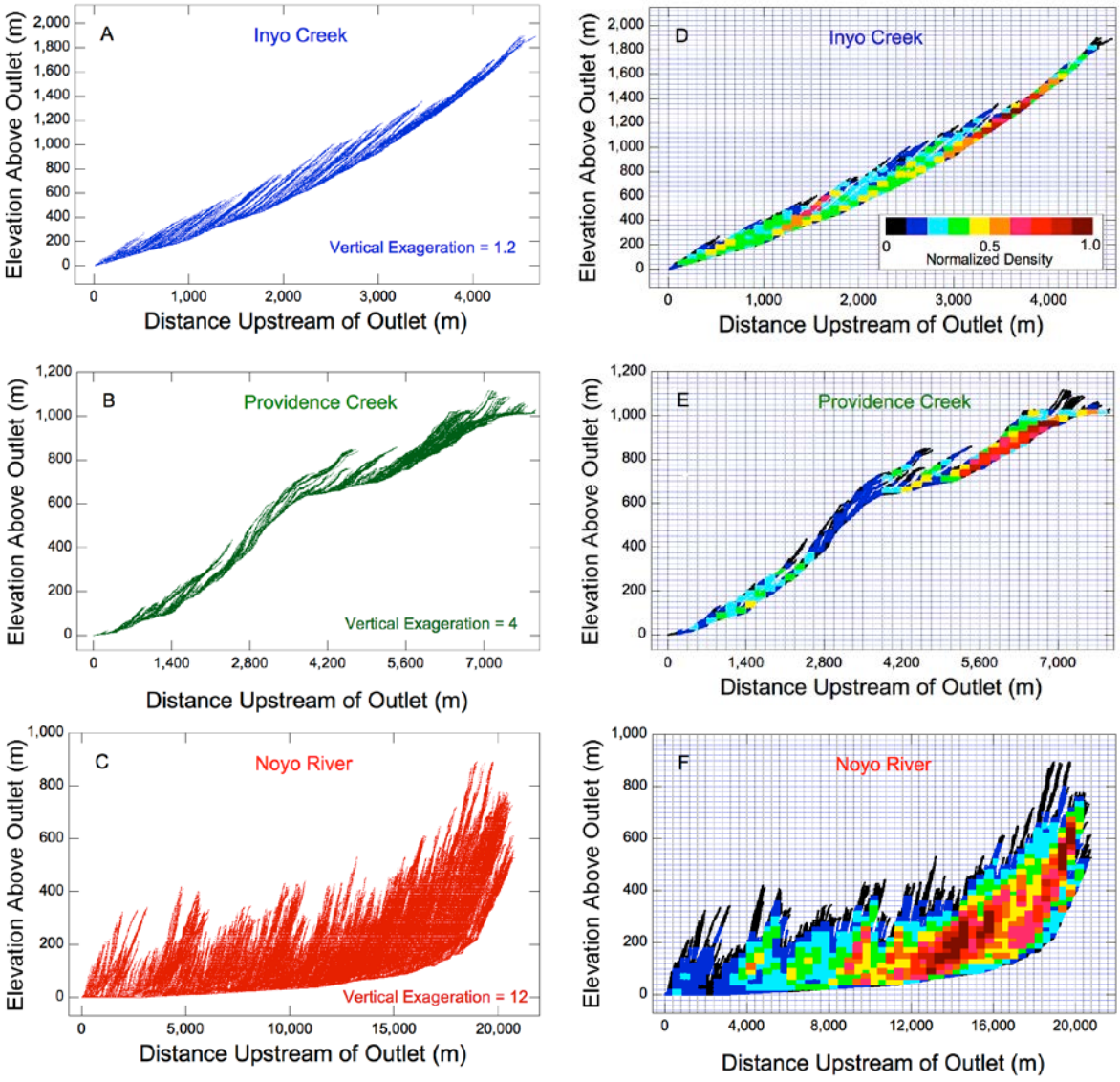

Figure 4. Joint distributions of elevation and travel distance. Distribution of source area elevations and travel distances from 10 m DEMs of catchments drained by (a) Inyo Creek, (b) Providence Creek, and (c) the Noyo River. Bivariate frequency distributions of elevation and travel distance for each catchment (d-f) show relative density (color bar in (d); data binning as in Figure 2.

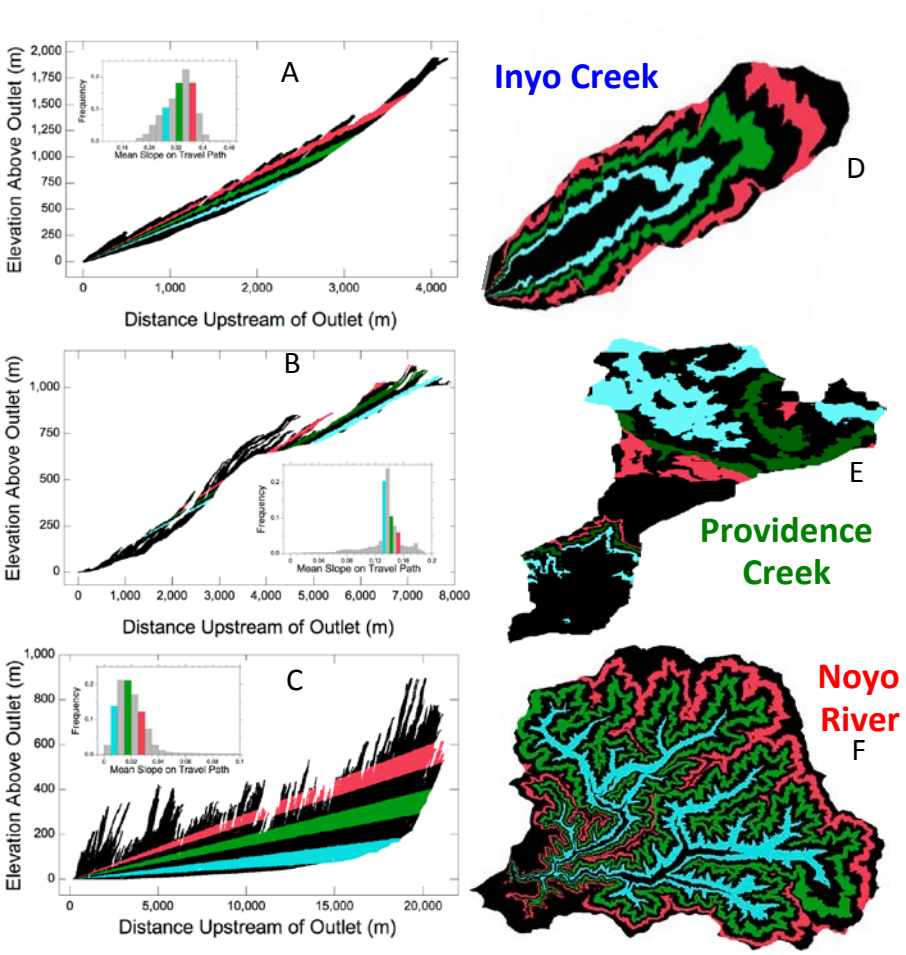

Figure 5. Distribution of mean slope across catchments. Histograms (insets, A-C) of mean slope along travel path from source to outlet (ratio of source area elevation to travel distance), with colors highlighting bins of relatively low, medium and high values. Bins of common mean slope form linear bands on plots of elevation versus travel distance (A-C). Maps of catchments (D-F) show spatial distribution of source areas sharing similar mean slope for highlighted values.

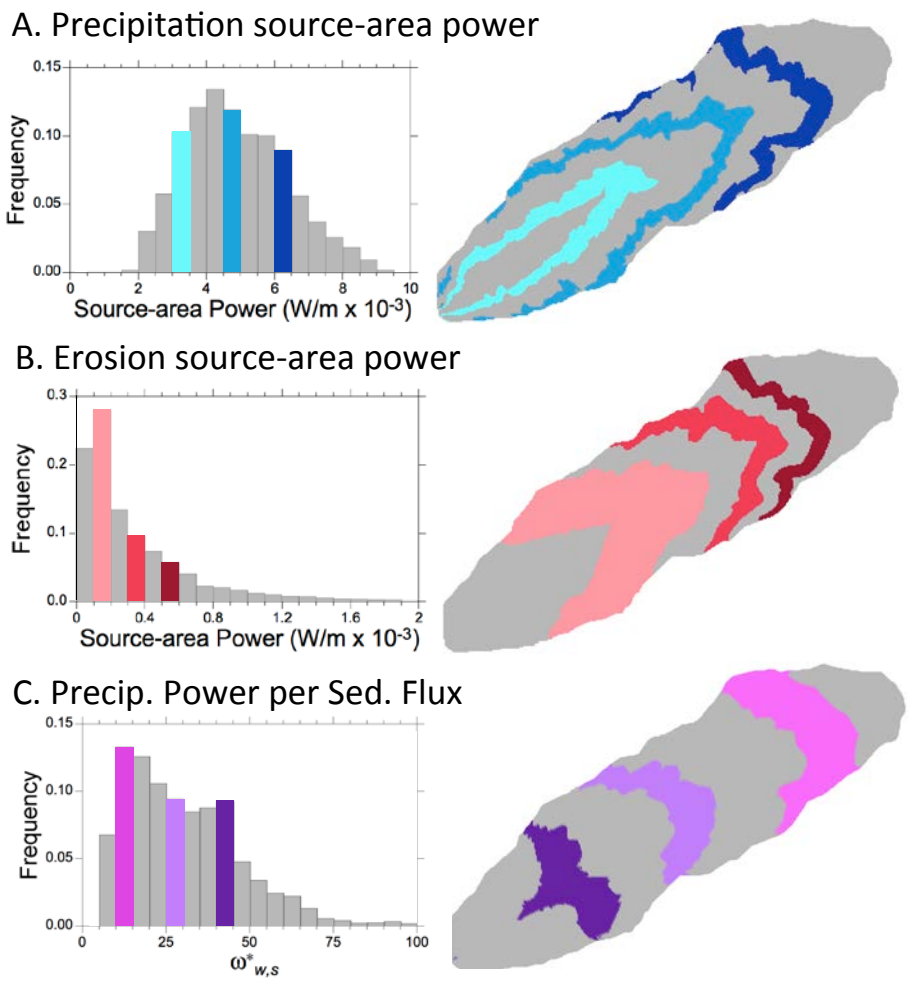

Figure 6. Spatial distribution of source-area power for water and sediment. Histograms (left) of source-area power calculated using equation 3 for the Inyo Creek catchment for water delivered by precipitation (A), and sediment produced by erosion (B). Panel (C) shows dimensionless ratio of source-area water power to sediment production rate (eqn. 4); colors highlight bins of relatively low, medium and high values. Maps (right) show spatial distribution of highlighted values. Note the sharp increase in water power per sediment flux from upper to lower parts of the catchment.

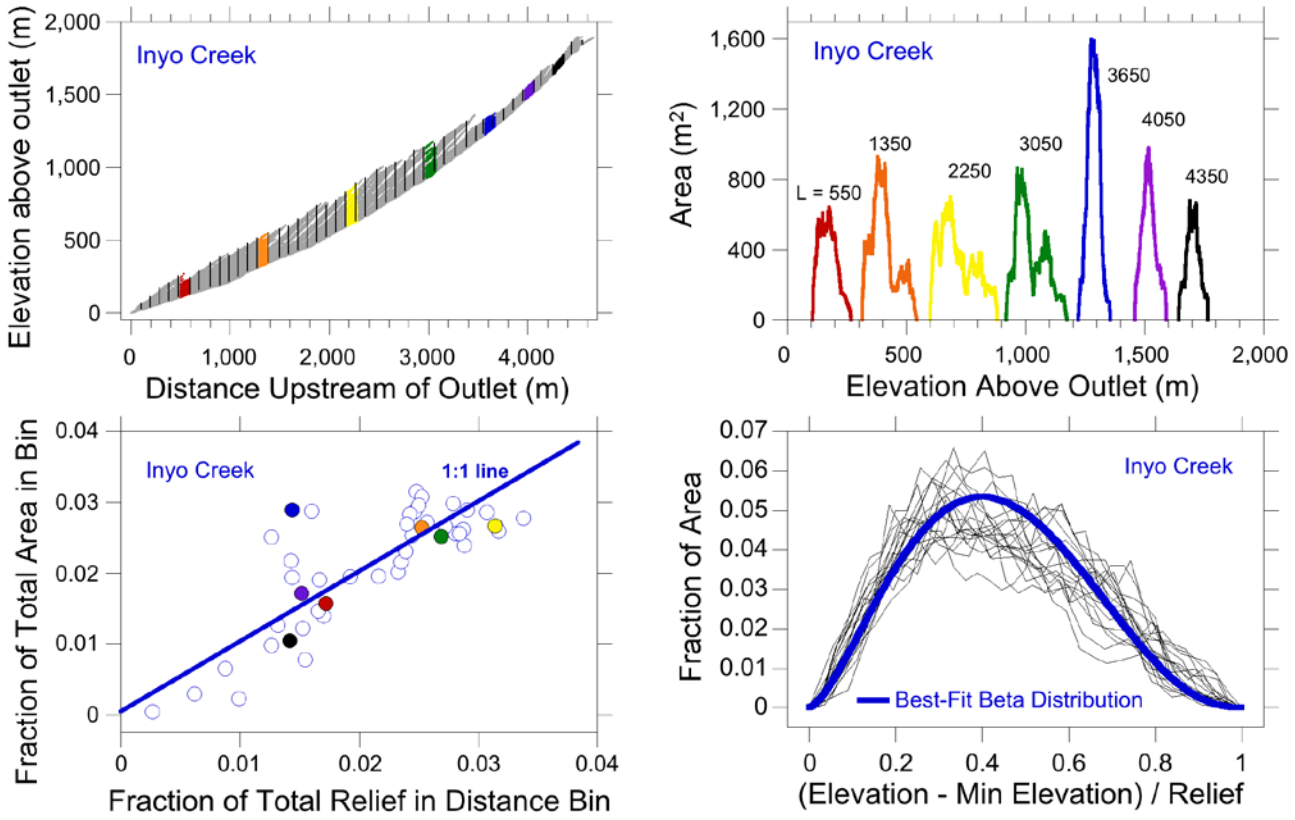

Figure 7. Elevation distributions for different travel distances at Inyo Creek
(A) Elevation data points for Inyo Creek catchment parsed into forty seven 100-m wide travel distance bins. (B) Distributions of elevation for seven representative travel distance bins; colors correspond to shaded bins in panel A, mean travel distance indicated for each curve. (C) Fraction of total area in each travel distance bin as a function of fraction of total relief in each bin, roughly follows 1:1 line, colored symbols indicate representative bins in panels A and B. (D) Collapse of elevation distributions for each travel distance bin, with elevation binned in 40 m increments. Elevation is normalized by total relief within distance bin and area normalized by total area within bin. Best-fit beta distribution captures typical shape of hypsometry for a given travel distance.

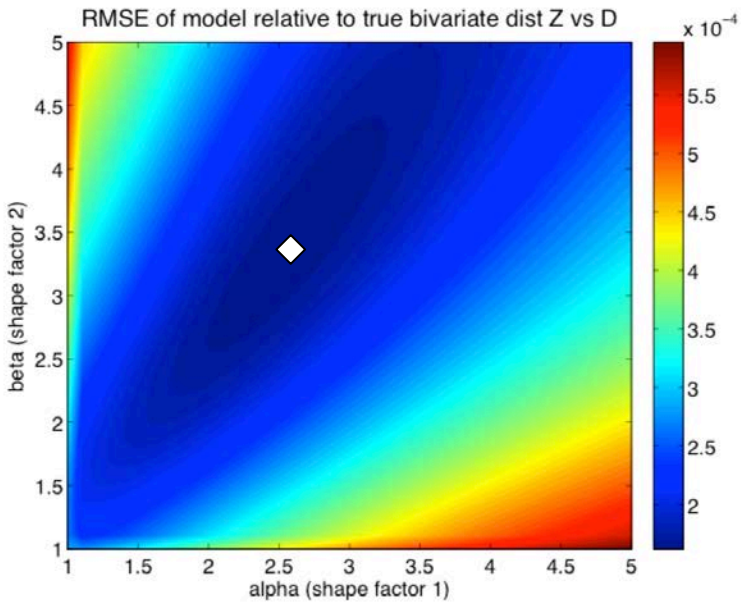

Figure 8. Objective function for best-fit beta distribution shape parameters. Contour plot of root mean sum of squared error (RMSE) between actual and predicted area density of elevation for a given travel distance for paired values of beta distribution shape parameters. Minimum RMSE at $\alpha = 2.6$ and $\beta = 3.4$ as indicated by open diamond. In this example, travel distance and elevation bin sizes equal 100 m and 40 m respectively.

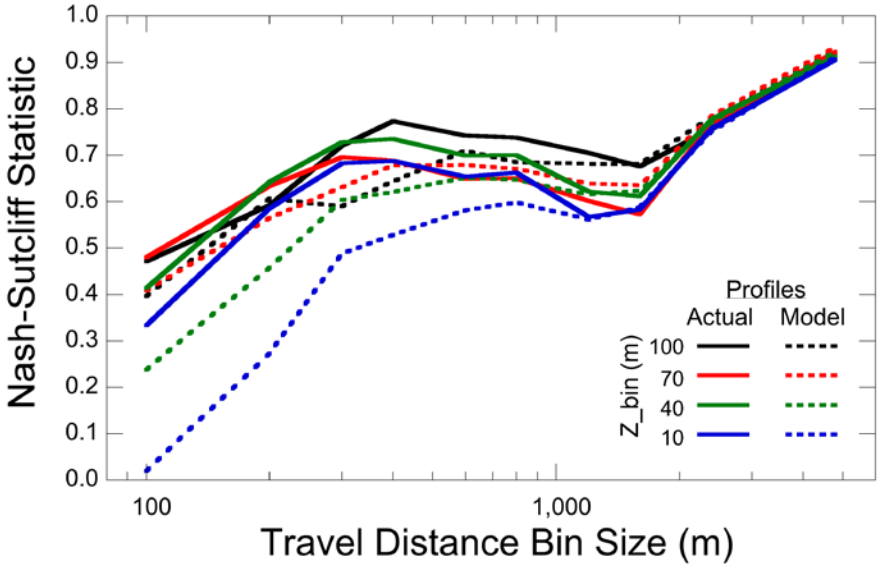

Figure 9. Model performance. Variation in Nash-Sutcliff model efficiency statistic with size of travel distance and elevation bins, for modeled joint distributions of elevation and travel distance for Inyo Creek, using actual profiles (solid lines) and modeled profiles (dashed lines). Nash-Sutcliff value of 1.0 indicates perfect agreement between modeled and actual distribution of area; value of 0 indicates model performance no better than uniform distribution of mean area density. A trade-off between model efficiency and spatial resolution is revealed by trend toward higher Nash-Sutcliff values for larger bin sizes.

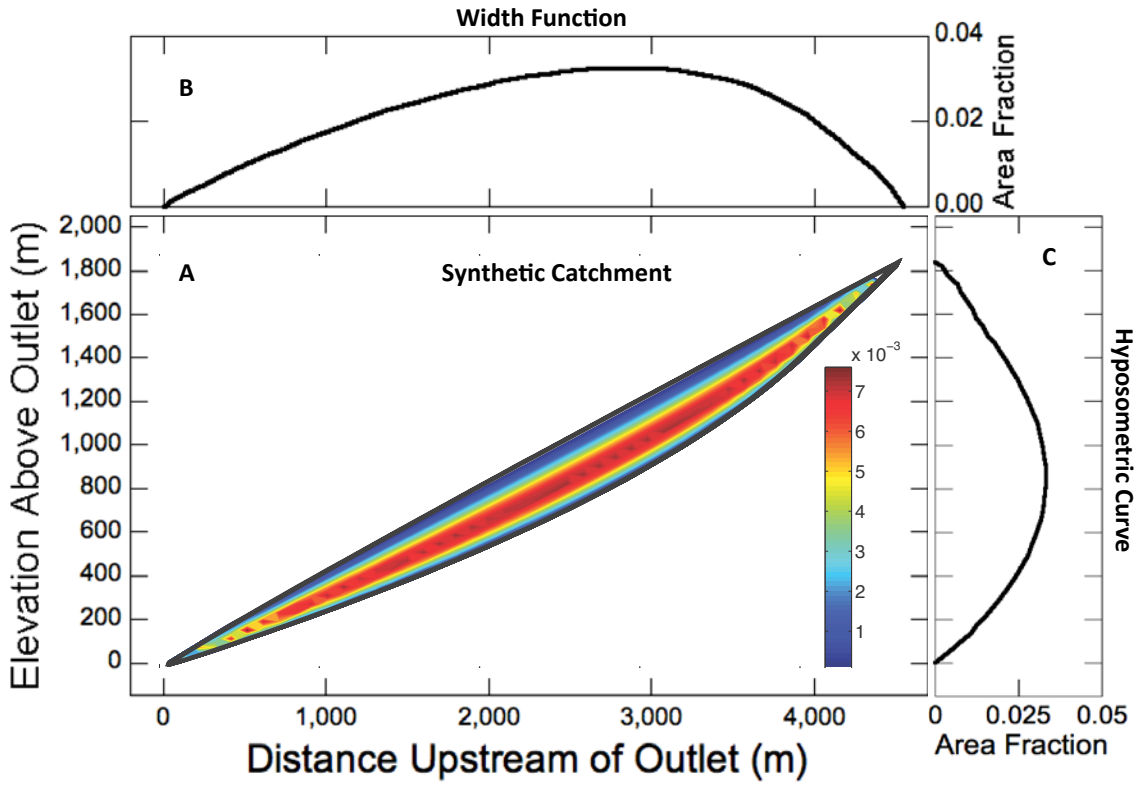

Figure 10. Fully synthetic joint distribution of elevation and travel distance for catchment the size of Inyo Creek. In (A) channel and ridge profiles are defined by equations 9 and 10, area density (color bar) given by equations 7 and 11. Side panels show area density projected on distance axis to create width function (B) and projected on elevation axis to create hypsometric curve (C).

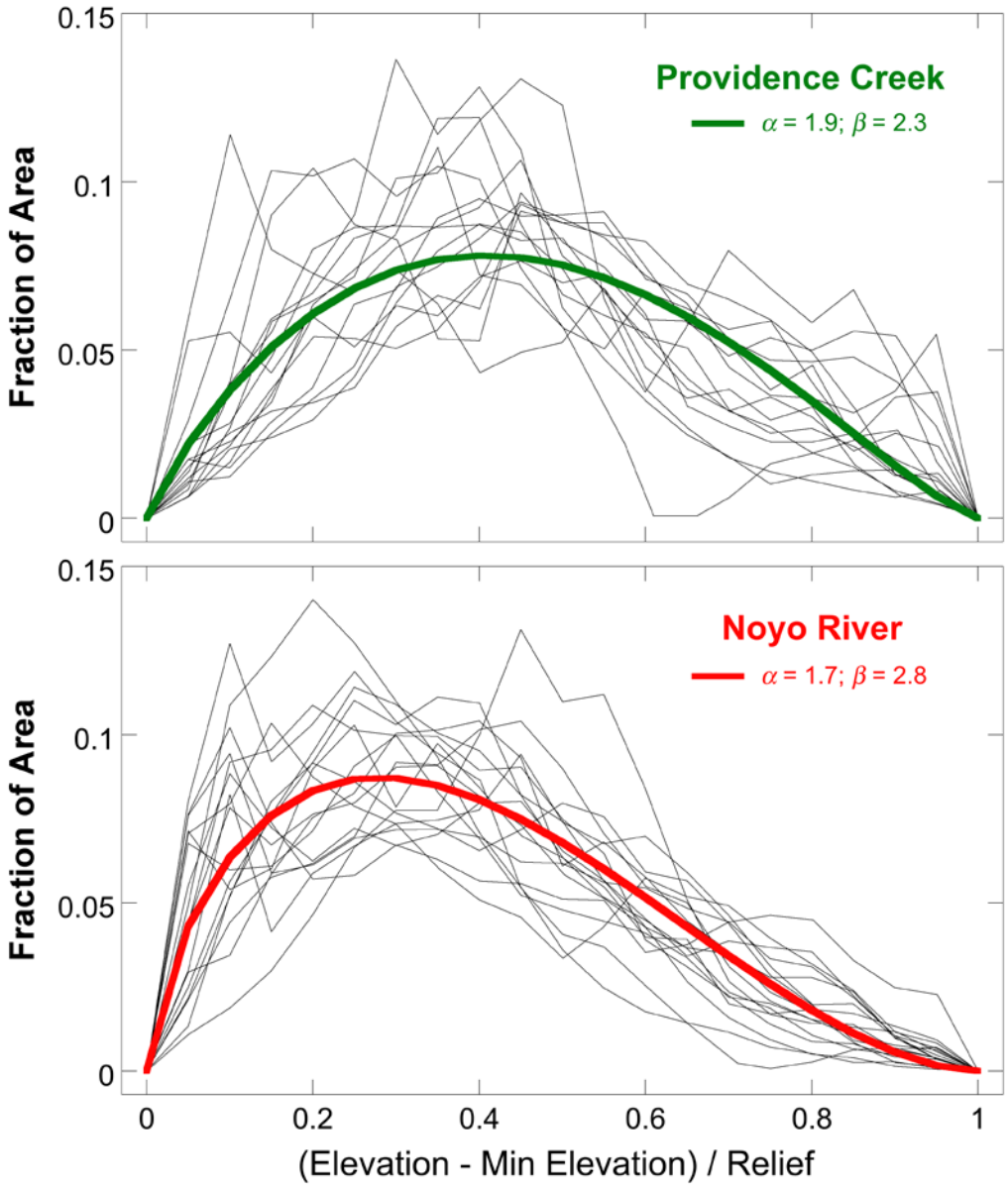

Figure 11. Normalized Distribution of elevation by travel distance bin for other catchments. Travel distance and elevation bin sizes = 1/20 of maximum values Thin lines show elevation distributions, normalized by local relief, for each travel distance bin. Thick colored curves show best-fit beta distributions, with shape parameter values indicated. Normalized elevation distributions are more skewed for Noyo River, reflecting larger drainage area and greater degree of landscape dissection.

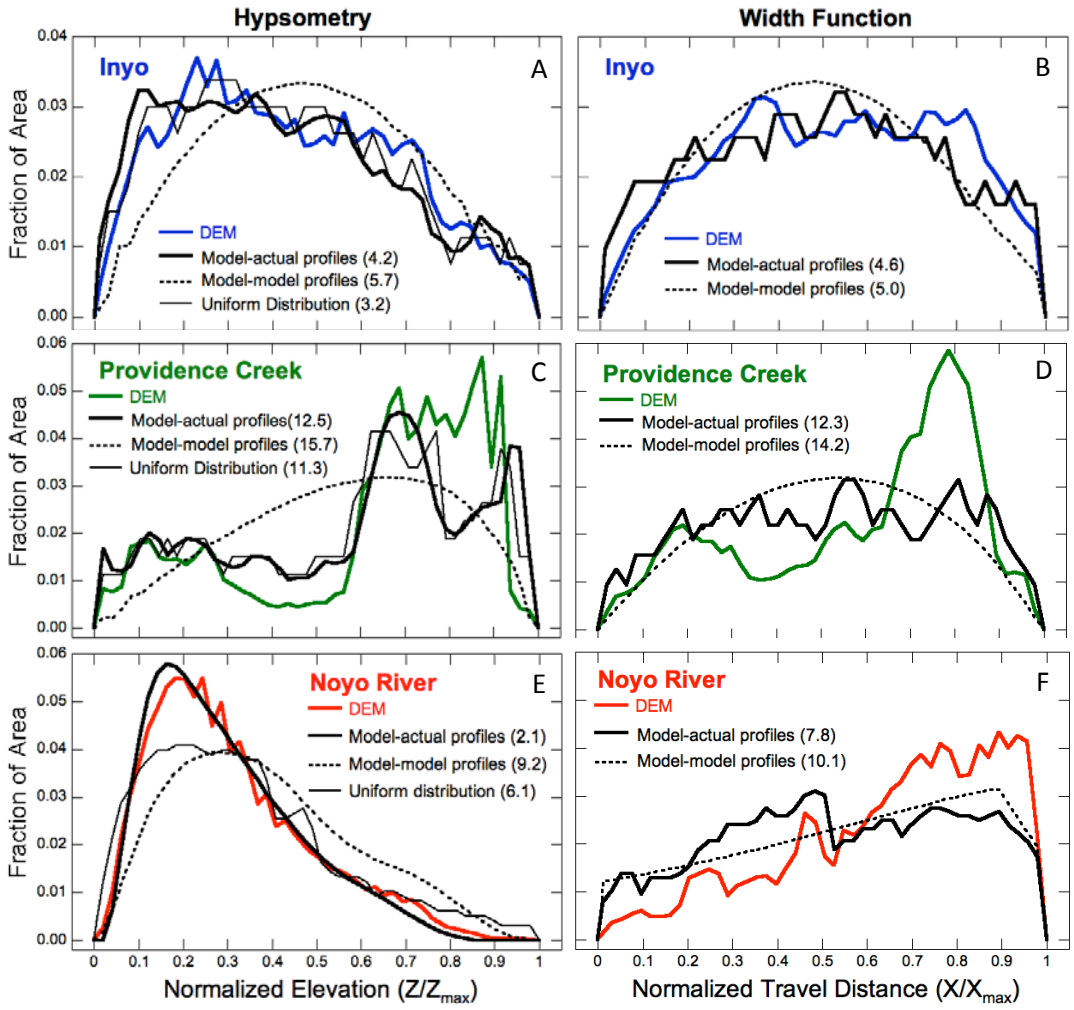

Figure 12. Comparison of actual with modeled hypsometric curves and width functions for three study catchments. In each panel, thick colored curves show data from catchment DEM, while thick and dashed black lines show model predictions using actual and modeled channel and ridge profiles respectively. Also shown in left panels are hypsometric curves predicted using uniform area distribution, for the case when Nash-Sutcliff model efficiency statistic = 0; for this case, predicted width function matches actual. Values in parenthesis indicate RMSE calculated by comparing model curves with DEM.